The eyes reflect an internal cognitive state embedded in the population activity of cortical neurons

Richard Johnston[1, 2, 3], Adam C. Snyder[4, 5, 6], Sanjeev B. Khanna[3, 7], Deepa Issar[1] and Matthew A. Smith[1, 2, 3]

[1]Department of Biomedical Engineering, Carnegie Mellon University, Pittsburgh, USA; [2]Neuroscience Institute, Carnegie Mellon University, Pittsburgh, USA; [3]Center for the Neural Basis of Cognition, Carnegie Mellon University, Pittsburgh, USA; [4]Department of Brain and Cognitive Sciences, University of Rochester, Rochester, USA; [5]Department of Neuroscience, University of Rochester, Rochester, USA; [6]Center for Visual Science, University of Rochester, Rochester, USA; [7] Department of Bioengineering, University of Pittsburgh, Pittsburgh, USA.

Corresponding author:
Matthew A. Smith, PhD
Carnegie Mellon University
Department of Biomedical Engineering and Neuroscience Institute
Mellon Institute, Room 115
Pittsburgh, PA 15213
Email: mattsmith@cmu.edu

Summary

Decades of research have shown that global brain states such as arousal can be indexed by measuring the properties of the eyes. Neural signals from individual neurons, populations of neurons, and field potentials measured throughout much of the brain have been associated with the size of the pupil, small fixational eye movements, and vigor in saccadic eye movements. However, precisely because the eyes have been associated with modulation of neural activity across the brain, and many different kinds of measurements of the eyes have been made across studies, it has been difficult to clearly isolate how internal states affect the behavior of the eyes, and vice versa. Recent work in our laboratory identified a latent dimension of neural activity in macaque visual cortex on the timescale of minutes to tens of minutes. This 'slow drift' was associated with perceptual performance on an orientation-change detection task, as well as neural activity in visual and prefrontal cortex (PFC), suggesting it might reflect a shift in a global brain state. This motivated us to ask if the neural signature of this internal state is correlated with the action of the eyes in different behavioral tasks. We recorded from visual cortex (V4) while monkeys performed a change detection task, and the prefrontal cortex, while they performed a memory-guided saccade task. On both tasks, slow drift was associated with a pattern that is indicative of changes in arousal level over time. When pupil size was large, and the subjects were in a heighted state of arousal, microsaccade rate and reaction time decreased while saccade velocity increased. These results show that the action of the eyes is associated with a dominant mode of neural activity that is pervasive and task-independent, and can be accessed in the population activity of neurons across the cortex.

Introduction

In the fields of psychology and neuroscience, the eyes are often viewed as a window to the brain. Much has been learned about cognitive processes, and their development, from studying the action of the eyes [1–7]. In addition, a large body of research has shown that properties related to the eyes can be used to index global brain states such as arousal, motivation and cognitive effort [8–13]. The action of the eyes can be considered broadly in two contexts – the action of the pupil when the eyes are relatively stable, and the action of the eyes when they move, be it voluntarily, in response to novel objects in the visual field, or involuntarily during periods of steady fixation. In each context, technological advancements in infrared eye-tracking have allowed rich insight about a subject's global brain state to be surmised in a rapid, accurate and non-invasive manner [14,15].

When the eyes are relatively stable, the size of the pupil changes in response to the amount of light hitting the retina [16]. However, the pupil does not merely reflect accommodation. Instead, the size of the pupil is controlled by a balance between parasympathetic and sympathetic pathways that reflect both light-driven accommodation and central modulation [12]. Several studies have shown that pupil size is associated with arousal [9–13]. In the mammalian brain, arousal has been largely associated with the activity of the locus coeruleus (LC) [17–22]. This small structure in the pons contains a dense population of noradrenergic neurons and is the primary source of norepinephrine (NE) to the central nervous system [23–25]. Recent neurophysiological work carried out in rodents and non-human primates has shown that pupil size is significantly associated with the spiking responses of LC neurons [23,26–28]. Under conditions of heightened arousal, increases in LC activity and NE concentration are accompanied by increases in pupil size [17–22].

Voluntary saccades occur ~3 times per second to bring novel objects onto the high-resolution fovea [29]. The characteristics of these saccades, such as the reaction time to initiate the saccade, and the velocity reached during the saccade, have similarly been used to index global changes in arousal [8]. For example, when arousal is increased by delivering a startling auditory stimulus prior to the execution of a saccade, reaction time decreases and saccade velocity increases [31–34]. Another metric that has been linked to global brain states, although to a lesser extent than reaction time and saccade velocity, is microsaccade rate. These small involuntary saccades are generated at a rate of 1-2Hz through the activity of neurons in the superior colliculus (SC) [34–37]. Evidence suggests that microsaccade rate decreases with increased cognitive effort on a range of behavioral tasks [38–41]. Taken together, these results suggest that the action of the eyes, be it when they are relatively stable and when they move, can be used to index global brain states.

A number of studies have related the activity of single neurons in many regions of the brain to pupil size [26,42], microsaccade rate [43–49], reaction time [50–55] and saccade velocity [56,57]. However, if changes in these eye metrics are driven by a shift in an underlying internal state, then one might expect them all to be related to a common underlying neural activity pattern. Recent work in our laboratory used dimensionality reduction to identify a dominant mode of neural activity called slow drift that was related to behavior in a change detection task and present in both visual and prefrontal cortex in the macaque [58]. If such a prevalent change in brain-wide neural activity was truly reflective of a changing internal state, then it might also be reflective of wide-ranging changes in behavior. This motivated us to ask if our measure of the brain's internal state ("slow drift") is related to the activity of the eyes in different behavioral tasks. We recorded the spiking responses of populations of neurons in V4 while monkeys performed a change detection task and PFC while the same subjects performed a memory-guided saccade task. On both tasks,

slow drift was associated with a pattern that is indicative of changes in the subjects' arousal level over time. When pupil size increased, microsaccade rate and reaction time decreased while saccade velocity increased. These results show that the collective action of the eyes is associated with a dimension of neural activity that is pervasive and task-independent. They support the view that slow drift indexes a global brain state that manifests in the movement of the eyes and the size of the pupil.

Results

To determine if observation of the eyes could provide insight into the internal state associated with slow drift, we recorded the spiking responses of populations of neurons in two macaque monkeys using 100-channel "Utah" arrays. We recorded from neurons in 1) V4 while the subjects performed an orientation-change detection task (Figure 1A); and 2) PFC while they performed a memory-guided saccade task (Figure 1B). Data from each task has been published previously [58,60]. However, the main goal of this study was to determine whether the neural population activity was related to eye metrics in a predictable manner across tasks. Four eye metrics were recorded during each session: pupil size, microsaccade rate, reaction time and saccade velocity. These metrics were chosen because they have been used extensively to index global changes in brain state [8–11], and can be measured easily and accurately with an infrared eye tracker. We made each of these four measurements on every trial of both behavioral tasks (Figure 1).

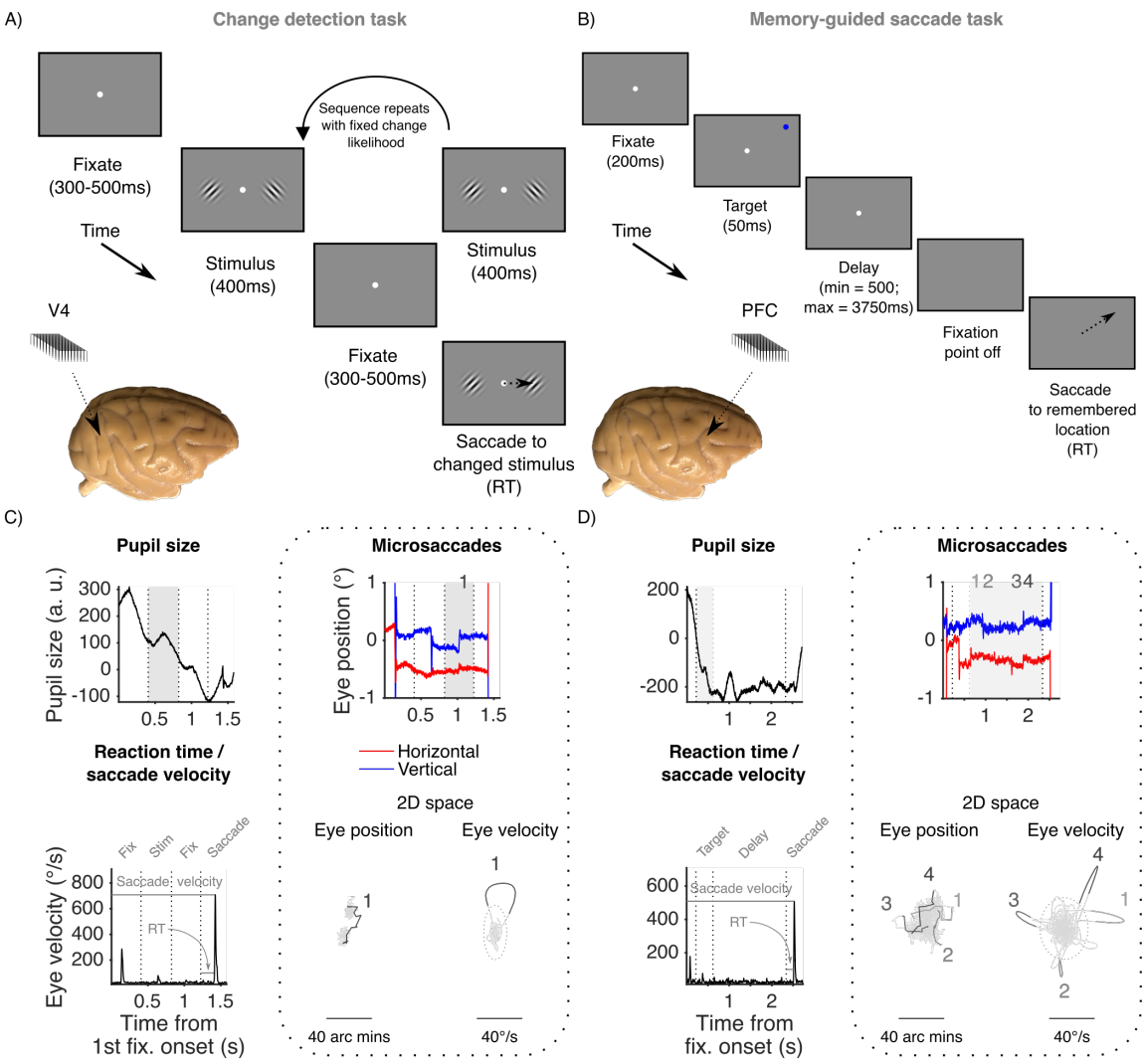

Figure 1. Experimental methods. (A) Change detection task. After an initial fixation period, a sequence of stimuli (orientated Gabors separated by fixation periods) was presented. The subjects' task was to detect an orientation change in one of the stimuli and make a saccade to the changed stimulus. We recorded neural activity from V4 while the animals performed the change detection task using 100-channel "Utah" arrays (inset). (B) Memory-guided saccade task. After an initial fixation period, a target stimulus was presented at 1 of 40 locations followed by a delay period. The central point was then extinguished prompting the subjects to make a saccade to the remembered target location. Neural activity was recorded in PFC while the animals performed the memory-guided saccade task using Utah arrays (inset). (C) Measuring eye metrics on the change detection task. Mean pupil size was recorded during stimulus periods, whereas microsaccade rate was measured during periods of steady fixation (except for the initial fixation period, see *Methods*). Microsaccades (emboldened in two-dimensional eye position and eye velocity space) were defined as eye movements that exceeded a threshold (dashed circle) for 6ms [103]. Reaction time was the time taken to make a saccade to the changed stimulus. Saccade velocity was the peak velocity of the saccade. (D) Measuring eye metrics on the memory-guided saccade task. Mean pupil size was recorded during the presentation of the target stimulus, whereas microsaccade rate was measured during the delay period. Reaction time was the time taken to make a saccade to the remembered target location. Saccade velocity was the peak of velocity of the saccade. RT = reaction time.

137 Correlations between the eye metrics over time

138 First, we investigated if the different measures of the eyes were themselves correlated over
139 time during performance of the behavioral task. A large body of work has shown that arousal is
140 associated with changes in the action of the eyes, be it when they are relatively stable or when they
141 move. For example, increases in arousal are typically accompanied by increases in pupil size and
142 saccade velocity, and concomitant decreases in microsaccade rate and reaction time [8–13,30–
143 33,38–41]. Given that arousal is a domain-general phenomenon, one might expect a similar pattern
144 to emerge on different behavioral tasks. To explore whether or not this was the case, we binned
145 our eye data using a 30-minute sliding window stepped every 6 minutes (Figure 2A and Figure
146 2B). The width of the window, and the step size, were chosen to isolate slow changes over time
147 based on previous research. They were the same as those used by Cowley et al. [58], which meant
148 direct comparisons could be made across studies. An example session from the same subject on
149 the change detection task and the memory-guided saccade task is shown in Figure 2C and Figure
150 2D, respectively. In the example sessions shown across both tasks a characteristic pattern was
151 observed that was indicative of slow changes in the subject's arousal level over time. Specifically,
152 a large tonic pupil size (measured during stimulus periods on the change detection task and target
153 presentations on the memory-guided saccade task) was associated with high saccade velocity,
154 shorter reaction times, and a lower rate of microsaccades.

155

156

157

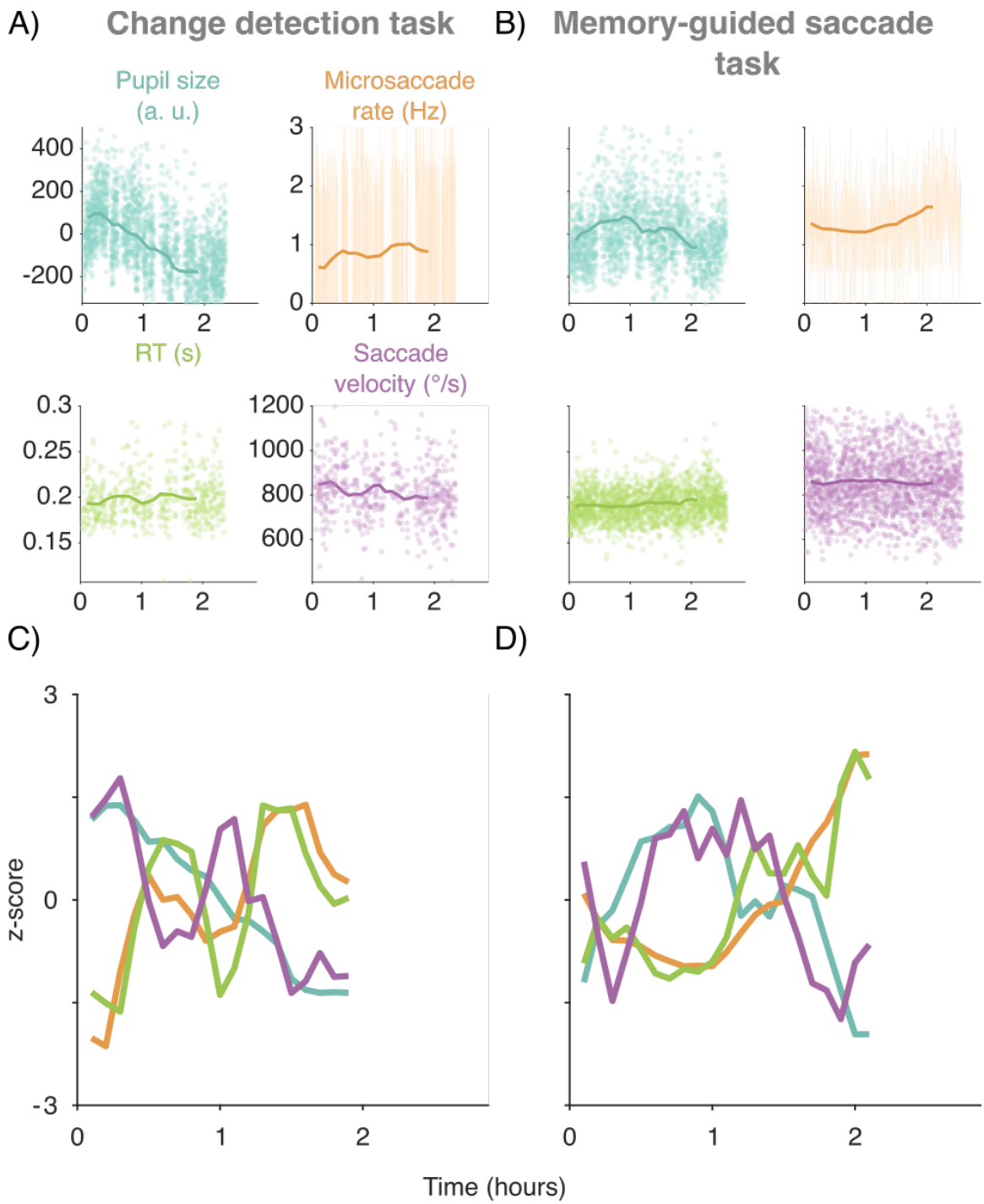

Figure 2. Isolating slow fluctuations in the eye metrics. (A) Change detection task. Each data point corresponds to a measurement from a single trial. To isolate slow changes, the data was binned using a 30-minute sliding window stepped every 6 minutes (solid line) [58]. (B) Same as (A) but for the memory-guided saccade task. Note in (B) and (C) that data points with a SD ~3 times greater than the mean are not shown for illustration purposes. (C) Example session from Monkey 1 on the change detection task. Each metric has been z-scored for illustration purposes. (D) Example session from the same subject on the memory-guided saccade task.

Next, we explored if a similar pattern was found across all sessions and both animals. We computed correlations (Pearson product-moment correlation coefficient) between all combinations of the four eye metrics for each session, and compared that distribution of Pearson's r values to shuffled distributions using permutation tests (two-sided, difference of medians). Consistent with the pattern of results observed in several individual sessions (Figure S5A and Figure S6A), we found significant interactions among the four eye metrics. Pupil size was significantly and negatively correlated with microsaccade rate (median $r = -0.46$; $p < 0.001$) and reaction time (median $r = -0.18$; $p = 0.027$) on the change detection task (Figure 3A and Figure S5B) and memory-guided saccade task (Figure 3B and Figure S6B, median $r = -0.56$; $p < 0.001$ for microsaccade rate and median $r = -0.15$; $p = 0.011$ for reaction time). We did not observe significant across-session trends in the correlation between pupil size and saccade velocity (change detection task: $r = 0.03$, $p = 0.651$; memory-guided saccade task: $r = 0.09$, $p = 0.523$ in Figure 3A-B), although saccade velocity was itself correlated with reaction time in both tasks (change detection task: $r = -0.52$, $p < 0.001$; memory-guided saccade task: $r = -0.61$, $p < 0.001$). Taken together, these results demonstrate that changes in the subjects' arousal level were accompanied by changes in the action of the eyes. This was true of pupil size, microsaccade rate, reaction time, and to a lesser extent, saccade velocity, and suggests that these eye metrics may be used to index global changes in brain state. This motivated us to ask next whether there were neural correlates of these behavioral signatures.

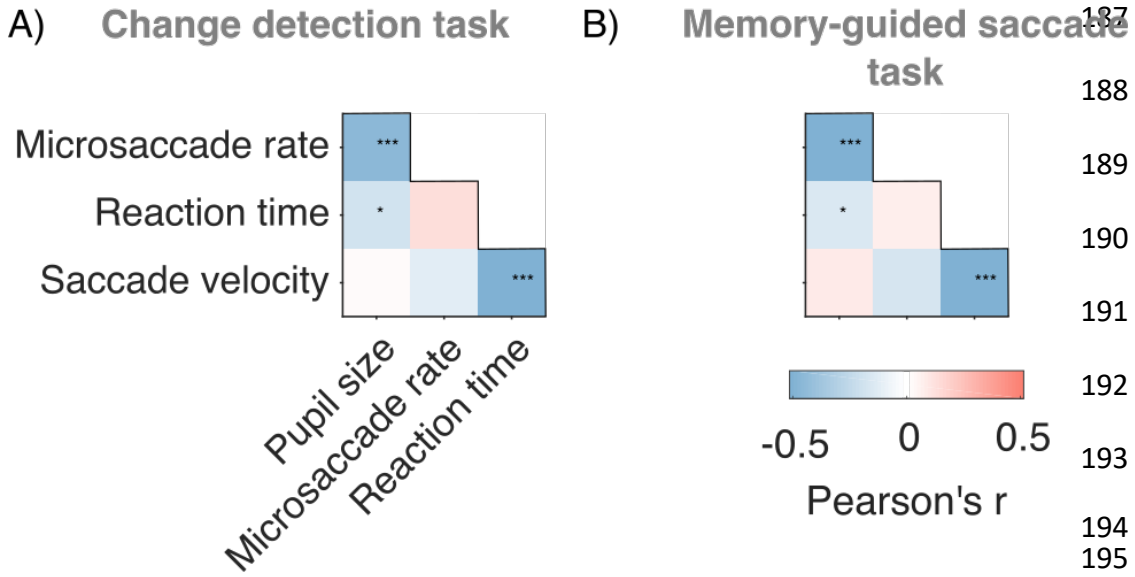

Figure 3. Correlations between the eye metrics over time. (A) Change detection task. Correlation matrix showing median r values across sessions between the four eye metrics. (B) Same as (A) but for the memory-guided saccade task. In (A) and (B) actual distributions of r values were compared to shuffled distributions using two-sided permutation tests (difference of medians). $p < 0.05$*, $p < 0.01$**, $p < 0.001$***.

<u>Correlation between the eye metrics and slow drift over time</u>

Previously we reported a slow fluctuation in neural activity in V4 and PFC that we termed 'slow drift' [58]. We found that this neural signature was related to the subject's tendency to make impulsive decisions in a change detection task, ignoring sensory evidence (false alarms). Here, we wanted to investigate if the constellation of eye metrics we observed were associated with the neural signature of internal state that we termed 'slow drift.' To calculate slow drift, we binned spike counts in V4 (change detection task) and PFC (memory-guided saccade task) using the same 30-minute sliding window that had been used to bin the eye metric data (Figure 4A-B, see *Methods*). We then applied principal component analysis (PCA) to the data and estimated slow drift by projecting the binned residual spike counts along the first principal component (i.e., the

212 loading vector that explained the most variance in the data). Because the sign of the loadings in
213 PCA is arbitrary [61], the correlation between slow drift and a given eye metric in any session was
214 equally likely to be positive or negative. This was problematic since we were interested in whether
215 slow drift was associated with a characteristic pattern that is indicative of changes in the subjects'
216 arousal level over time i.e., increased pupil size and saccade velocity, and decreased microsaccade
217 rate and reaction time. In order to establish consistency across sessions in the sign of the
218 correlations, we constrained the slow drift in each session to have the same relationship to the
219 spontaneous (change detection task = fixation periods; memory-guided saccade task = delay
220 periods) and evoked (change detection task = stimulus periods; memory-guided saccade task =
221 target presentations) activity of the neurons (Figure S4, and see *Methods*). This served to align
222 slow drift across sessions such that an increase in the slow drift value was associated with neural
223 activity closer to the evoked pattern of response (i.e., typically higher firing rates).

224 We computed the slow drift of the neuronal population in each session using this method,
225 and then compared it to the four eye measures. An example session is shown in Figure 4C-D for
226 the same subject on the change detection task and the memory-guided saccade task, respectively
227 (same sessions as in Figure 2). On both tasks, we found a characteristic pattern in which slow drift
228 was positively associated with pupil diameter and saccade velocity, and negatively associated with
229 microsaccade rate and reaction time.

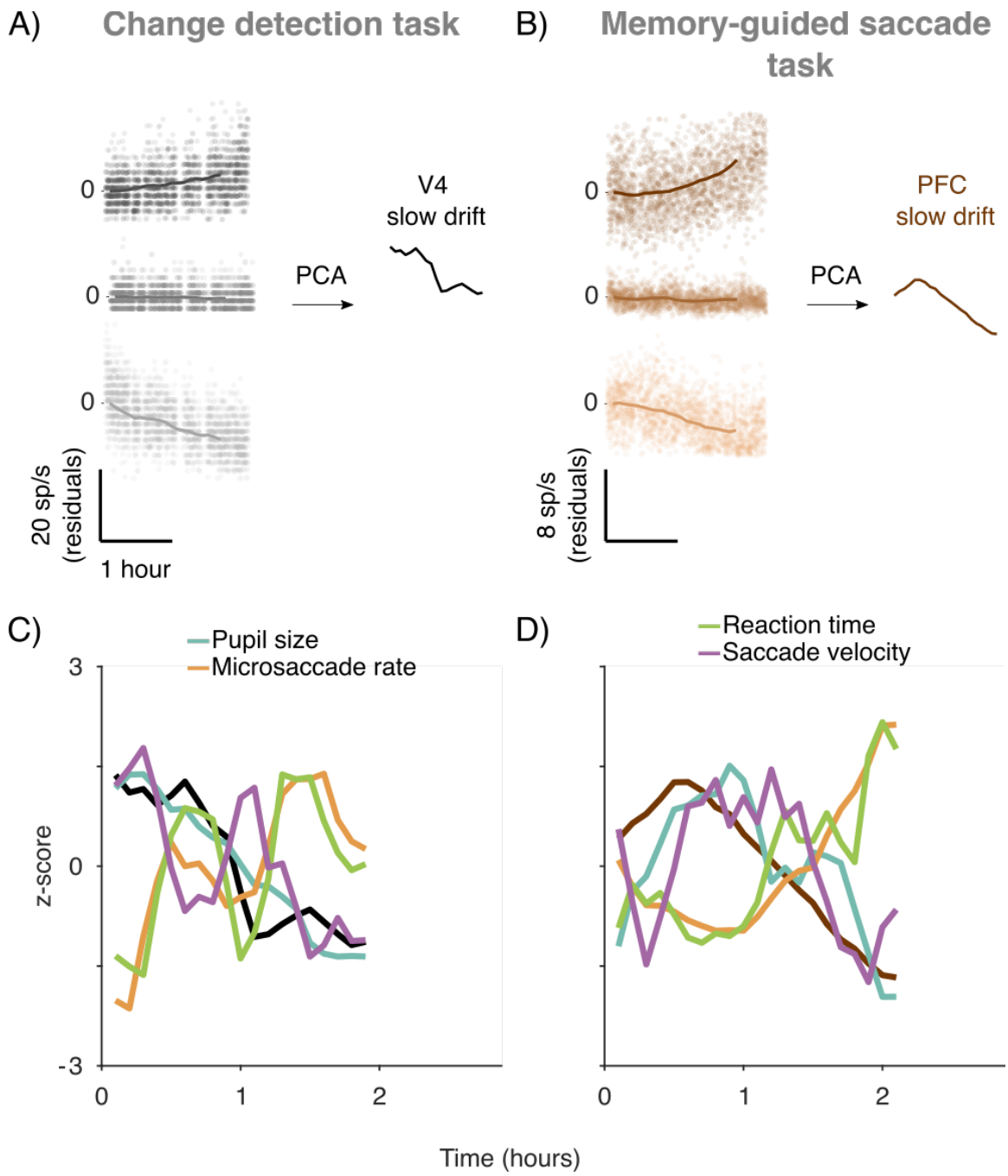

Figure 4. Calculating slow drift. (A) Change detection task. Three example neurons from a single session (Monkey 1). Each point represents the mean residual spike count during a 400ms stimulus period. The data was then binned using a 30-minute sliding window stepped every six minutes (solid line) so that direct comparisons could be made with the eye metrics. PCA was used to reduce the dimensionality of the data and slow drift was calculated by projecting binned residual spike counts along the first principal component. (B) Same as (A) but for the memory-guided saccade task (same subject). (C) Example session from Monkey 1 on the change detection task. Each metric has been z-scored for illustration purposes. (D) Example session from the same subject on the memory-guided saccade task.

Next, we explored if a similar pattern was found across sessions. We computed correlations (Pearson product-moment correlation coefficient) between slow drift and the eye metrics. Actual distributions of r values were then compared to shuffled distributions using permutation tests (two-sided, difference of medians). Because the slow drift was aligned across sessions based on the neural activity alone and not the behavior, the shuffled distributions are centered on a correlation value of zero. Consistent with the pattern of results observed in several individual sessions (Figure S7), we found that slow drift in V4 on the change detection task (Figure 5A) was positively correlated with pupil diameter (median $r = 0.46$, $p < 0.001$) and saccade velocity (median $r = 0.26$, $p < 0.001$), and negatively correlated with microsaccade rate (median $r = -0.28$, $p = 0.007$) and reaction time (median $r = -0.19$, $p = 0.016$). An identical pattern of results was found on the memory-guided saccade task (Figure 5B), where slow drift in PFC was positively correlated with pupil diameter (median $r = 0.20$; $p = 0.029$) and saccade velocity (median $r = 0.17$, $p = 0.042$), and negatively correlated with microsaccade rate (median $r = -0.42$; $p < 0.001$) and reaction time (median $r = -0.27$; $p = 0.008$). These results show that pupil size, microsaccade rate, reaction time and saccade velocity are associated with slow drift across tasks. Thus, the slow drift was associated with a pattern that is indicative of changes in the subject's arousal levels over time.

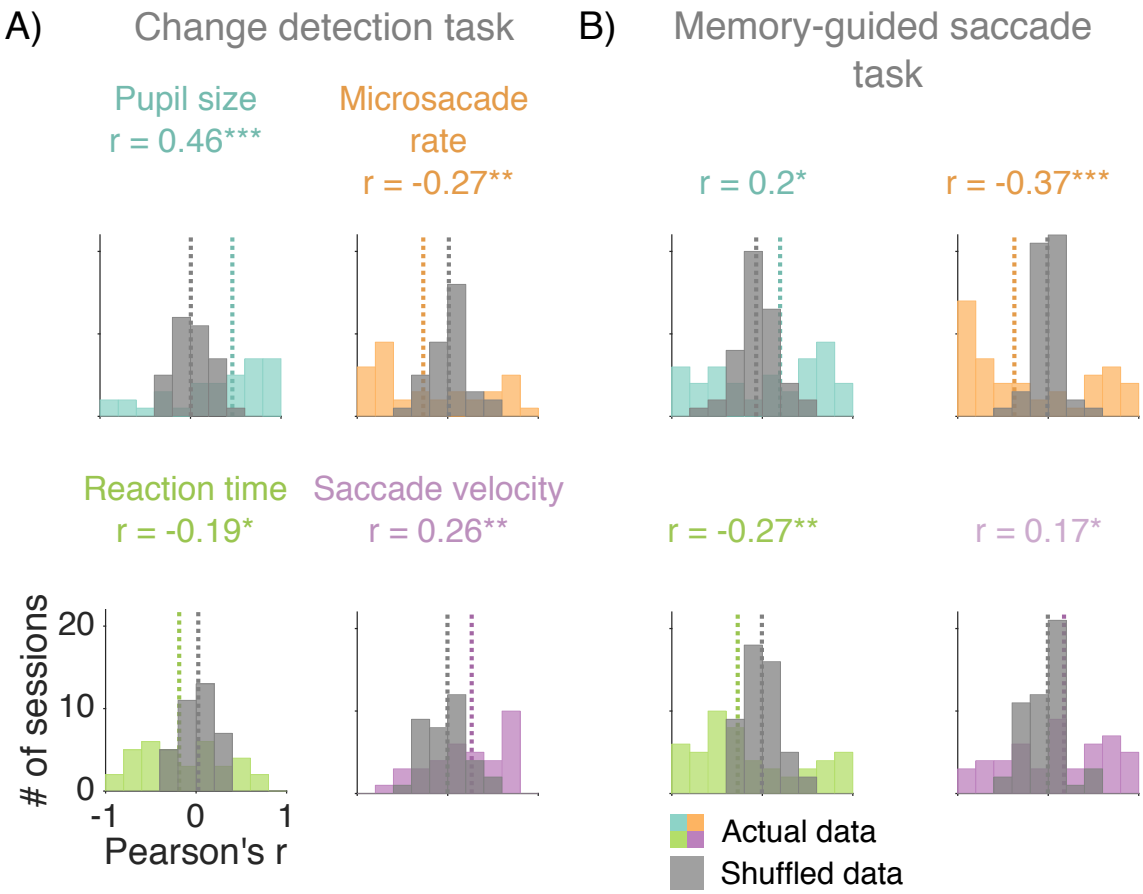

Figure 5. Correlations between the eye metrics and slow drift over time. (A) Change detection task. Histograms showing actual and shuffled distributions of r values. (B) Same as (A) but for the memory-guided saccade task. In (A) and (B) median r values across sessions are indicated by dashed lines (colored lines = actual data; gray lines = shuffled data). Actual distributions of r values were compared to shuffled distributions using two-sided permutation tests (difference of medians). $p < 0.05$*, $p < 0.01$**, $p < 0.001$***.

Discussion

In this study, we investigated if the size of the pupil and the movement of the eyes could be taken as an external signature of an internal brain state, a low-dimensional neural activity pattern called slow drift [58]. There is strong evidence that internal brain states such as slow drift can be measured in the population spiking activity of neurons, and that measurements of the eyes can provide important context into the behavior of subjects on perceptual and decision-making tasks. Hence, we were keen to determine whether we could directly link a neural measure of internal brain state acquired from the spiking activity of a population of neurons with external features of

behavior. On two types of perceptual tasks, we found that slow drift was significantly correlated with a pattern of eye metrics that was indicative of changes in the subjects' arousal level over time. Our results show that the action of the eyes, be it when they are relatively stable or when they move, is associated with a latent dimension of neural activity that is pervasive and task-independent.

As described above, decades of research have shown that eye metrics are related to task performance in a variety of contexts [8–13]. Heightened levels of arousal have been associated with a large pupil. In a variety of work, the size of the pupil has been associated positively with saccade velocity and negatively with microsaccade rate and reaction time [8–13,30–33,38–41]. Given that arousal is a global phenomenon, one might expect a common pattern across multiple behavioral tasks. In the present study, we addressed this issue by investigating the relationships between eye metrics on tasks designed to probe the mechanisms underlying perceptual decision making (change detection task) and working memory (memory-guided saccade task). Results showed that pupil size was negatively correlated with microsaccade rate and reaction time on both tasks. Although no significant correlation was found between pupil size and saccade velocity, the overall pattern of results suggests that each subject's arousal level was changing over time in a task-independent manner. These findings support the view that measuring properties related to the eyes can provide a non-invasive index of global brain states [8–13]. This motivated us to ask if they are also associated with slow drift.

Most studies that have explored the relationship between eye metrics and neural activity have used single-neuron (spike count, Fano factor) and pairwise statistics (r_{sc}). However, numerous recent studies have shown that rich insight about cognitive processes (e.g., learning, decision making, working memory, time perception) can be gained from analysis of the simultaneous

activity of populations of neurons [51,62–68]. In addition, recent work has shown that a low-dimensional representation of neural activity in the mouse can be used to index global changes in brain state. Stringer et al. [69] applied PCA to data recorded from more than 10,000 neurons and found that fluctuations in the first principal component were significantly associated with whisking, pupil size, and running speed. In this study, we investigated if slow drift, a dominant mode of neural activity in macaque cortex is associated with the action of the eyes. On both tasks, we found that it was correlated with a pattern of eye metrics that is indicative of changes in the subject's arousal level over time. Our results, coupled with those of Stringer et al. [69], suggest that much can be learned about global brain states, as well as cognitive processes, when high-dimensional population activity is reduced to a low-dimensional subspace [70–73]. A key question for future research is whether latent dimensions of neural activity in the cortex are associated with activity in subcortical brain regions? One might expect this to be the case given that slow drift was significantly correlated with pupil size on both tasks.

Evidence suggests that pupil size is associated with activity in the LC, a subcortical structure that regulates arousal by releasing NE in a diverse manner throughout much of the brain [74–77]. That slow drift can be used to index global brain states suggests that it might be associated with LC activity. Although the LC is limited in size (~3mm caudorostrally) and buried deep within the brainstem [78,79], several studies have successfully recorded from single neurons in LC of the macaque [26,27,80–84]. In addition, LC can be activated using optogenetics [85–88], electrical microstimulation [14,16, 58], and pharmacological manipulations [17,89,90]. Thus, it should be possible to alter the course of slow drift in the cortex using some, if not all, of these methods. As well as having a significant effect on pupil size, our results predict that activating the LC, directly

316 or indirectly, may lead to task-independent changes in microsaccade rate, reaction time and
317 saccade velocity.

318 Evidence suggests that microsaccades, reaction time and saccade velocity are associated
319 with neural activity in the SC [37]. This layered structure, located at the roof of the brain stem,
320 plays a critical role in transforming sensory information into eye movement commands. Population
321 recordings have been successfully performed in the SC using linear probes [91], and it thus might
322 be possible to identify dominant patterns of neural activity in SC using dimensionality reduction
323 [71]. Our results predict that slow drift in the cortex should be significantly correlated with slow
324 drift in the SC. However, this might depend upon the mixture of SC neurons in the recorded
325 population. We previously suggested that slow drift must be removed at some stage before motor
326 commands are issued to prevent unwanted eye movements [58]. Thus, one might not expect a
327 correlation between slow drift in the cortex and slow drift in deep-layer SC neurons that fire
328 vigorously prior to the execution of a saccade, and relay motor commands to downstream nuclei
329 innervating the oculomotor muscles [92]. An alternative possibility is that slow drift is not
330 removed, but instead occupies an orthogonal subspace in the SC that is not read out by downstream
331 nuclei. This is not beyond the realm of possibility given that an identical scheme appears to exist
332 in the skeletomotor system to stop preparatory signals reaching the muscles [93–96]. Further
333 research is needed to disentangle these possibilities.

334 Studies in the fields of psychology and neuroscience have mainly used pupil size to index
335 arousal, but metrics such as heart rate (HR) and galvanic skin response (GSR) are also associated
336 with global brain states. For example, Wang et al. [97] measured pupil size, HR and GSR while
337 human subjects viewed emotional face stimuli specifically designed to evoke fluctuations in
338 arousal. Results showed that all three metrics were positively correlated prior to the presentation

of the stimuli. That is, when pupil size was large, and the subjects were in heightened state of arousal, HR and GSR increased. In addition, it has been suggested that pre-stimulus oscillations in the alpha band can be used to index global brain states as they are inversely related to performance on visual detection tasks. Several studies using electroencephalography (EEG) have shown that the probability of detecting near-threshold stimuli increases when pre-stimulus power in the alpha band is low [98–101]. Simultaneous recordings of spiking activity and EEG in awake behaving monkeys are rare. However, our results predict that slow drift should be associated with pre-stimulus alpha oscillations.

Research has also uncovered a link between alpha oscillations and microsaccades [102]. This effect has been attributed to changes in spatial attention, which have a profound effect on microsaccade direction [106–110]. For example, Lowet et al. [49] found that attention-related modulation of spiking responses, Fano factor and r_{sc} only occur following a microsaccade in the direction of an attended stimulus [49]. In the present study, we found that slow drift was significantly correlated with microsaccade rate on both tasks. This is unlikely to be explained by changes in spatial attention as both Cowley et al. [58] and Rabinowitz et al. [109] found that slow drift on a change detection task was not associated with the blocks of trials used to cue spatial attention inside and outside the RF. In addition, the correlation between slow drift and microsaccade rate in the present study was lower on the change detection task ($r = -0.27$) than the memory-guided saccade task ($r = -0.37$). One would not have expected this to be the case if slow drift was mediated by changes in spatial attention. These results raise the possibility that spatial attention and arousal have differential effects on microsaccades. Attention might specifically affect microsaccade direction, whereas arousal might affect microsaccade rate irrespective of direction. Further research is needed to test this hypothesis.

362 In summary, we investigated if properties related to the eyes are associated with slow drift:
363 a low-dimensional pattern of neural activity that was recently identified in the macaque cortex by
364 Cowley et al. [58]. On both tasks, we found that slow drift was significantly associated with a
365 pattern of eye metrics that is indicative of changes in the subjects' arousal level over time. These
366 results demonstrate that the collective action of the eyes is associated with a latent dimension of
367 neural activity that is pervasive and task-independent. They suggest that slow drift can be used to
368 index global changes in brain state over time. Further research is necessary to determine the origins
369 of this slow drift in population activity. A key question for future work will be to determine the
370 mechanisms by which slow drift influences behavior in some instances (e.g., when arousal level
371 drives an urgent response) and is circumvented in others (e.g., when an accurate perceptual
372 judgement must be made regardless of arousal level).

373 Methods

374 Subjects

375 Two adult rhesus macaque monkeys (*Macaca mulatta*) were used in this study. Surgical
376 procedures to chronically implant a titanium head post (to immobilize the subjects' head during
377 experiments) and microelectrode arrays were conducted in aseptic conditions under isoflurane
378 anesthesia, as described in detail by Smith and Sommer [108]. Opiate analgesics were used to
379 minimize pain and discomfort during the perioperative period. Neural activity was recorded using
380 100-channel "Utah" arrays (Blackrock Microsystems) in V4 (Monkey 1 = right hemisphere;
381 Monkey 2 = left hemisphere) and PFC (Monkey 1 = right hemisphere; Monkey 2 = left
382 hemisphere) while the subjects performed the change detection task (Figure 1A). On the memory-
383 guided saccade task (Figure 1B), neural activity was only recorded in PFC (Monkey 1 = left
384 hemisphere; Monkey 2 = right hemisphere). The arrays comprised a 10x10 grid of silicon

385 microelectrodes (1 mm in length) spaced 400 μm apart. Experimental procedures were approved
386 by the Institutional Animal Care and Use Committee of the University of Pittsburgh and were
387 performed in accordance with the United States National Research Council's Guide for the Care
388 and Use of Laboratory Animals.

389 Microelectrode array recordings

390 Signals from each microelectrode in the array were amplified and band-pass filtered (0.3–
391 7500 Hz) by a Grapevine system (Ripple). Waveform segments crossing a threshold (set as a
392 multiple of the root mean square noise on each channel) were digitized (30KHz) and stored for
393 offline analysis and sorting. First, waveforms were automatically sorted using a competitive
394 mixture decomposition method [110]. They were then manually refined using custom time
395 amplitude window discrimination software ([111], code available at
396 https://github.com/smithlabvision/spikesort), which takes into account metrics including (but not
397 limited to) waveform shape and the distribution of interspike intervals. A mixture of single and
398 multiunit activity was recorded, but we refer here to all units as "neurons". On the change detection
399 task, the mean number of V4 neurons across sessions was 70 (SD = 11) for Monkey 1 and 31 (SD
400 = 16) for Monkey 2, whereas the mean number of PFC neurons across sessions was 84 (SD = 15)
401 for Monkey 1 and 90 (SD = 20) for Monkey 2. On the memory-guided saccade task, the mean
402 number of PFC neurons across sessions was 54 (SD = 11) for Monkey 1 and 38 (SD = 19) for
403 Monkey 2.

404 Visual stimuli

405 Visual stimuli were generated using a combination of custom software written in
406 MATLAB (The MathWorks) and Psychophysics Toolbox extensions (Brainard, 1997; Pelli, 1997;
407 Kleiner et al., 2007). They were displayed on a CRT monitor (resolution = 1024 X 768 pixels;

408 refresh rate = 100Hz), which was viewed at a distance of 36cm and gamma-corrected to linearize
409 the relationship between input voltage and output luminance using a photometer and look-up-
410 tables.

411 Behavioral tasks

412 Orientation-change detection task

413 Subjects fixated a central point (diameter = 0.6°) on the monitor to initiate a trial (Figure
414 1A). Each trial comprised a sequence of stimulus periods (400ms) separated by fixation periods
415 (duration drawn at random from a uniform distribution spanning 300-500ms). The 400ms stimulus
416 periods comprised pairs of drifting full-contrast Gabor stimuli. One stimulus was presented in the
417 aggregate receptive field (RF) of the recorded V4 neurons, whereas the other stimulus was
418 presented in the mirror-symmetric location in the opposite hemifield. Although the spatial
419 (Monkey 1 = 0.85cycles/°; Monkey 2 = 0.85cycles/°) and temporal frequencies (Monkey 1 =
420 8cycles/s; Monkey 2 = 7cycles/s) of the stimuli were not optimized for each individual V4 neuron
421 they did evoke a strong response from the population. The orientation of the stimulus in the
422 aggregate RF was chosen at random to be 45 or 135°, and the stimulus in the opposite hemifield
423 was assigned the other orientation. There was a fixed probability (Monkey 1 = 30%; Monkey 2 =
424 40%) that one of the Gabors would change orientation by ±1, ±3, ±6, or ±15° on each stimulus
425 presentation. The sequence continued until the subject) made a saccade to the changed stimulus
426 within 700ms ("hit"); 2) made a saccade to an unchanged stimulus ("false alarm"); or 3) remained
427 fixating for more than 700ms after a change occurred ("miss"). If the subject correctly detected an
428 orientation change, they received a liquid reward. In contrast, a time-out occurred if the subject
429 made a saccade to an unchanged stimulus delaying the beginning of the next trial by 1s. It is
430 important to note that the effects of spatial attention were also investigated (although not analyzed

431 in this study) by cueing blocks of trials such that the orientation change was 90% more likely to
432 occur within the aggregate V4 RF than the opposite hemifield. Data exploring how spatial attention
433 effects diversity in the neural population code [59] and slow drift [58] have been published
434 previously.

435 Memory-guided saccade task

436 Subjects fixated a central point (diameter = 0.6°) on the monitor to initiate a trial (Figure
437 1B). After fixating within a circular window (diameter = 2.4° and 1.8° for Monkey 1 and Monkey
438 2, respectively) for 200ms, a target stimulus (diameter = 0.8°) was presented for 50ms (except for
439 1 session in which it was presented for 400ms). The target stimulus appeared at 1 of 8 angles
440 separated by 45°, and 1 of 5 eccentricities, yielding 40 conditions in total. After the target stimulus
441 had been presented, subjects were required to maintain fixation for a delay period. For Monkey 1,
442 the duration of the delay period was either 1) drawn at random from a distribution spanning 1200-
443 3750ms; or 2) fixed at 1400 or 2000ms. For Monkey 2, the duration of the delay period was 500ms.
444 If steady fixation was maintained throughout the delay period, the central point was extinguished
445 prompting the subjects to make a saccade to the remembered target location. The subjects had
446 500ms to initiate a saccade. Once the saccade had been initiated, they had a further 200ms to reach
447 the remembered target location. To receive a liquid reward, the subjects' gaze had to be maintained
448 within a circular window centered on the target location (diameter = 4 and 2.7° for Monkey 1 and
449 Monkey 2, respectively) for 150 ms. In a subset of sessions, the target was briefly reilluminated,
450 after the fixation point was extinguished and the saccade had been initiated, to aid in saccade
451 completion.

452 Eye tracking

453 Eye position and pupil diameter were recorded monocularly at a rate of 1000Hz using an
454 infrared eye tracker (EyeLink 1000, SR Research).

455 Microsaccade detection

456 Microsaccades were defined as eye movements that exceeded a velocity threshold of 6
457 times the standard deviation of the median velocity for at least 6ms [103,114,115]. They were
458 required to be separated in time by at least 100ms. In addition, we removed microsaccades with
459 an amplitude greater than 1° and a velocity greater than 100°/s. To assess the validity of our
460 microsaccade detection method, the correlation (Pearson product-moment correlation coefficient)
461 between the amplitude and peak velocity of detected microsaccades (i.e., the main sequence) was
462 computed for each session (Figure S1A and Figure S1B). The mean correlation between
463 microsaccade amplitude and peak microsaccade velocity across sessions was 0.86 (SD = 0.07) for
464 the change detection task and 0.83 (SD = 0.04) for the memory-guide saccade task (Figure S1C
465 and Figure S1D). These findings indicate that our microsaccade detection algorithm was robust
466 [116].

467 Eye metrics

468 Change detection task

469 Mean pupil diameter was measured during stimulus periods, whereas microsaccade rate
470 was measured during fixation periods (Figure 1C). We did not include the first fixation period
471 when measuring microsaccade rate in the change-detection task. As can be seen in Figure 1C, there
472 was an increase in eye position variability during this period resulting from fixation having been
473 established a short time earlier (300-500ms). Such variability was not present in proceeding
474 fixation periods. Reaction time and saccade velocity were measured on trials in which the subjects
475 were rewarded for correctly detected an orientation change. Reaction time was defined as the time

476 from when the change occurred to the time at which the saccade exceeded a velocity threshold of
477 100°/s. Saccade velocity was the peak velocity of the saccade to the changed stimulus. To isolate
478 slow changes in the eye metrics over time the data for each session was binned using a 30-minute
479 sliding window stepped every 6 minutes (Figure 2A).

480 Memory-guided saccade task.

481 Pupil size, microsaccade rate, reaction time and saccade velocity were measured on trials
482 in which the subjects received a liquid reward for making a correct saccade to the remembered
483 target location. Mean pupil diameter was measured during the presentation of the target stimulus,
484 whereas microsaccade rate was measured during the delay period (Figure 1D). Reaction time was
485 defined as the time from when the fixation point was extinguished to the time at which the saccade
486 reached a threshold of 100 °/s. Saccade velocity was the peak of velocity of the saccade to the
487 remembered target location. As in the change-detection task, the data for each session was binned
488 using a 30-minute sliding window stepped every 6 minutes (Figure 2B).

489 Calculating slow drift

490 Orientation-change detection task

491 The spiking responses of populations of neurons in V4 were measured during a 400ms
492 period that began 50ms after stimulus presentation (Figure 4A). To control for the fact that some
493 neurons had a preference for one orientation (45 or 135°) over the other residual spike counts were
494 calculated. We subtracted the mean response for a given orientation across the entire session from
495 individual responses to that orientation. To isolate slow changes in neural activity over time,
496 residual spike counts for each V4 neuron were binned using a 30-minute sliding window stepped
497 every 6 minutes [58]. PCA was then performed to reduce the high-dimensional residual data to a
498 smaller number of variables [71]. Slow drift in V4 was estimated by projecting the binned residual

499 spike counts for each neuron along the first principal component [58]. As described above, the
500 spiking responses of neurons in PFC were simultaneously recorded on the change detection task.
501 When PFC slow drift was calculated using the method described above, we found it to be
502 significantly associated with V4 slow drift (median $r = 0.95$, $p < 0.001$), consistent with previous
503 results [58]. On the change detection task, we investigated the relationships between the eye
504 metrics and V4 slow drift. However, a very similar pattern of results was found when slow drift
505 was calculated using simultaneously recorded PFC data (Figure S2). The only difference was the
506 correlation between slow drift and reaction time, which was not statistically significant ($r = -0.09$,
507 $p = 0.495$).

508 Memory-guided saccade task

509 The spiking responses of populations of neurons in PFC were measured during the delay
510 period (Figure 4B). To control for the fact that some neurons had a preference for one target
511 location over another, residual spike counts were calculated. We subtracted the mean response to
512 a given target location across the entire session from individual responses to that location. To
513 isolate slow changes in neural activity over time residual spike counts for each PFC neuron were
514 binned using a 30-minute sliding window stepped every 6 minutes. PCA was then performed, and
515 slow drift was estimated by projecting the binned residual spike counts for each neuron along the
516 first principal component.

517 Controlling for neural recording instabilities

518 To rule out the possibility that slow drift arose due to recording instabilities (e.g., the
519 distance between the neuron and the microelectrodes changing slowly over time) we only included
520 neurons with stable waveform shapes throughout a session. This was quantified by calculating
521 percent waveform variance for each neuron (Figure S3). First, the session was divided into 10 non-

522 overlapping time bins. A residual waveform was then computed for each time bin by subtracting
523 the mean waveform across time bins. The variance of each residual waveform was divided by the
524 variance of the mean waveform across time bins yielding 10 values (one of reach time bin). Percent
525 waveform variance was defined as the maximum value across time bins. Neurons with a percent
526 waveform variance greater than 10% were deemed as having unstable waveform shapes
527 throughout a session. They were excluded from all analyses, consistent with previous research
528 [58].

529 Aligning slow drift across sessions

530 As described above, slow drift was calculated by projecting binned residual spike counts
531 along the first principal component [58]. The weights in a PCA can be positive or negative [61],
532 which meant the sign of the correlation between slow drift and a given eye metric was arbitrary.
533 Preserving the sign of the correlations was particularly important in this study because we were
534 interested in whether slow drift was associated with a pattern that is indicative of changes in the
535 subjects' arousal levels over time i.e., increased pupil size and saccade velocity, and decreased
536 microsaccade rate and reaction time. Thus, we had to devise a method to align slow drift across
537 sessions. As expected, the mean evoked population response calculated during stimulus periods
538 on the change detection task was significantly higher than the mean spontaneous population
539 response calculated during fixation periods (Figure S4A). Similarly, on the memory-guided
540 saccade task, the mean evoked population response calculated during target presentations was
541 significantly higher than the mean spontaneous population response calculated during delay
542 periods (Figure S4B). To align slow drift for each individual session, we projected evoked and
543 spontaneous responses onto the first principal component (Figure S4C-D). The sign of the slow
544 drift was flipped if the mean projection value for the evoked responses was less than that for the

spontaneous responses – i.e., if the relationship described above for unprojected data did not hold true.

Acknowledgements

D.I. was supported by National Institutes of Health (NIH) Grant T32 GM-008208 and the ARCS Foundation Thomas-Pittsburgh Chapter Award. M.A.S. was supported by NIH Grants R01 EY-022928, R01 MH-118929, R01 EB-026953, and P30 EY-008098; NSF Grant NCS 1734901; a career development grant and an unrestricted award from Research to Prevent Blindness; and the Eye and Ear Foundation of Pittsburgh. A.C.S. was supported by NIH grant K99EY025768. S.B.K. was supported by NIH Grant T32 EY-017271. The authors would like to thank Ms. Samantha Schmitt for assistance with surgery and data collection.

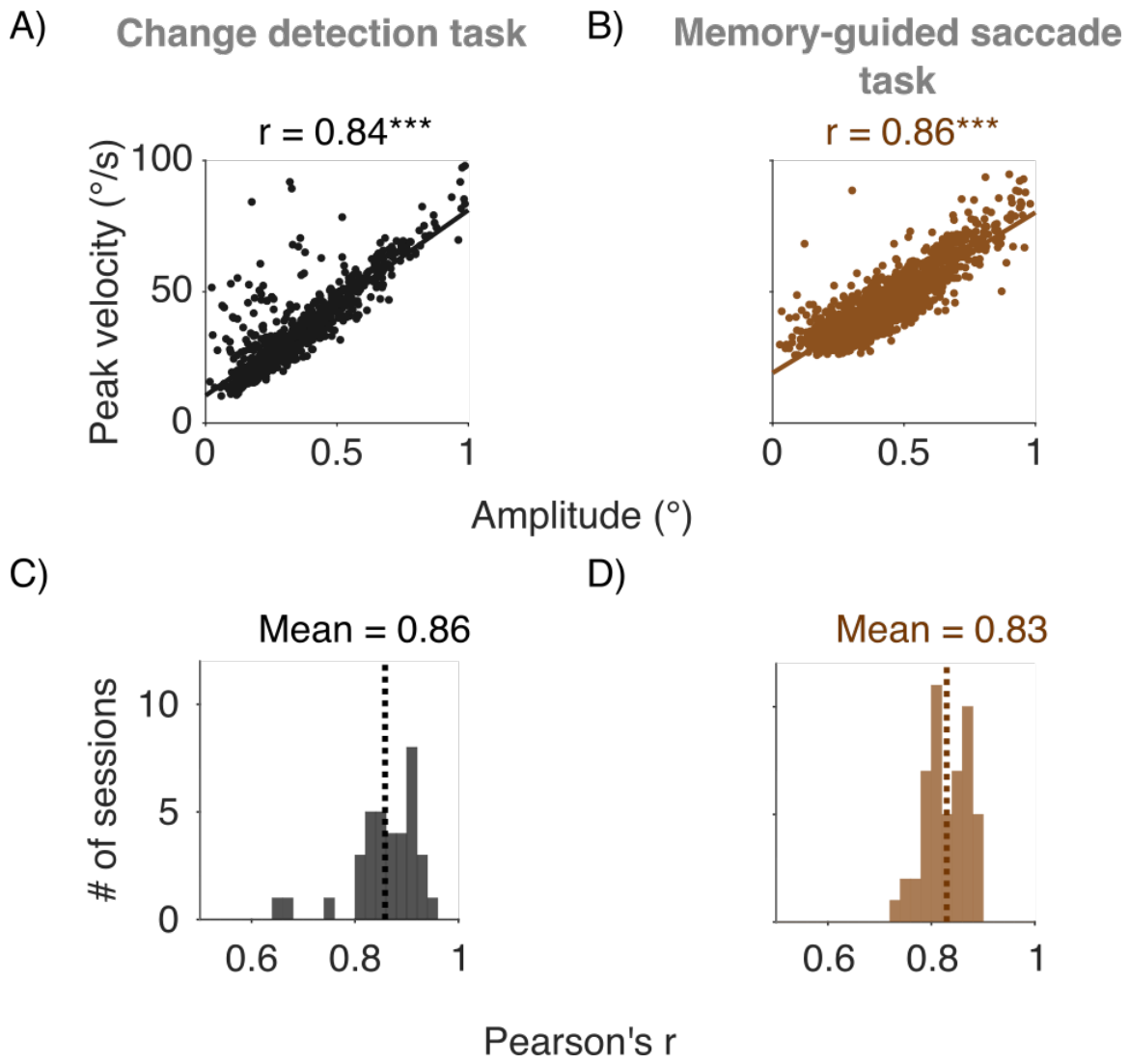

Figure S1. Assessing the validity of our microsaccade detection algorithm. The correlation between the amplitude and peak velocity of detected microsaccades was computed for each session. (A) Change detection task. Scatter plot showing the relationship between microsaccade amplitude and peak velocity for an example session on the change detection task. (B) Same as (A) but for the memory-guided saccade task (same subject). (C) Histogram showing the distribution of r values for the change detection task. (D) Same as (C) but for the memory-guided saccade task. In (C) and (D) dashed lines indicate the mean r value across sessions. On both tasks, the mean correlation between microsaccade amplitude and peak velocity was strong, indicating that our method of detecting microsaccades was robust [116]. $p < 0.05$*, $p < 0.01$**, $p < 0.001$***.

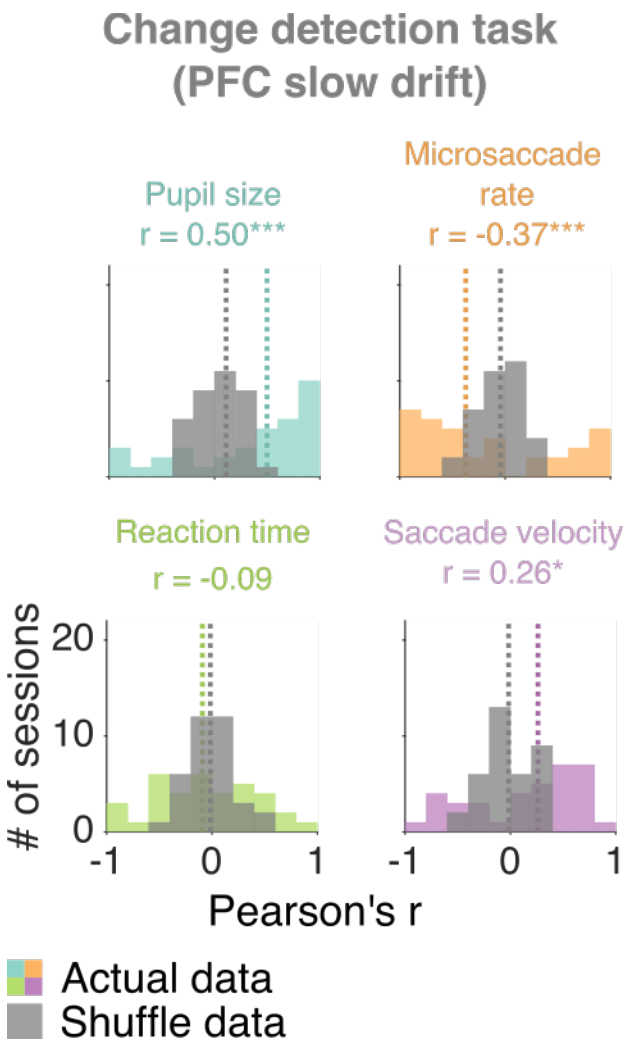

Figure S2. Correlations between the eye metrics and PFC slow drift on the change detection task. Histograms showing actual and shuffled distributions of r values. Median r values across sessions are indicated by dashed lines (colored lines = actual data; gray lines = shuffled data). Actual distributions of r values were compared to shuffled distributions using two-sided permutation tests (difference of medians). $P < 0.05$*, $p < 0.01$**, $p < 0.001$***.

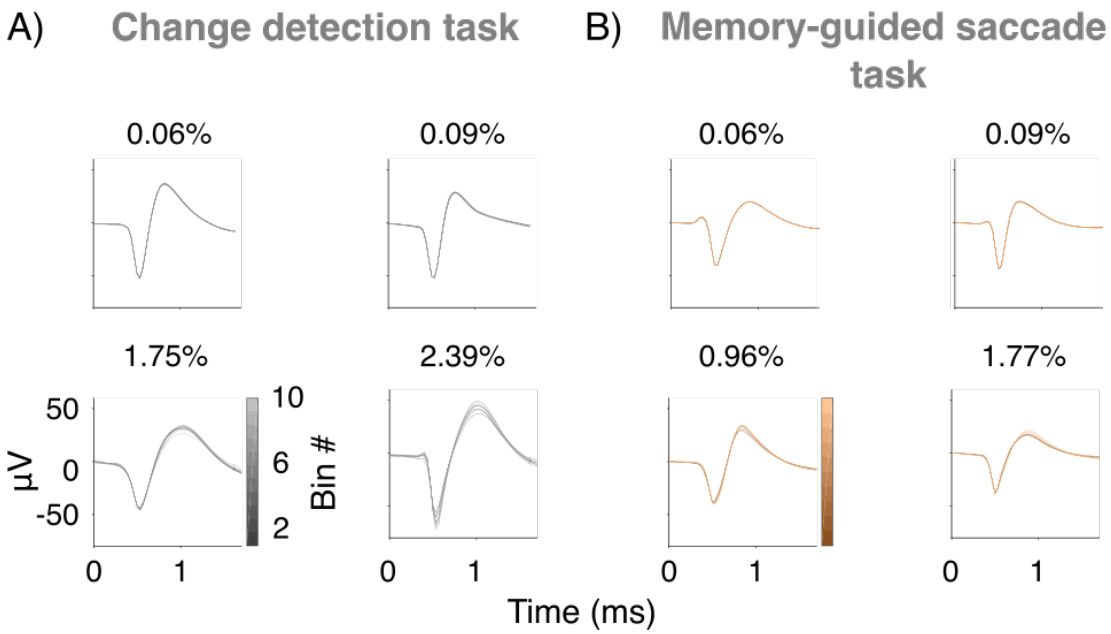

Figure S3. Controlling for neural recording instabilities. (A) Percent waveform variance of four example neurons recorded from Monkey 1 during a single session on the change detection task. (B) Same as (A) but for the memory-guided saccade task (same subject).

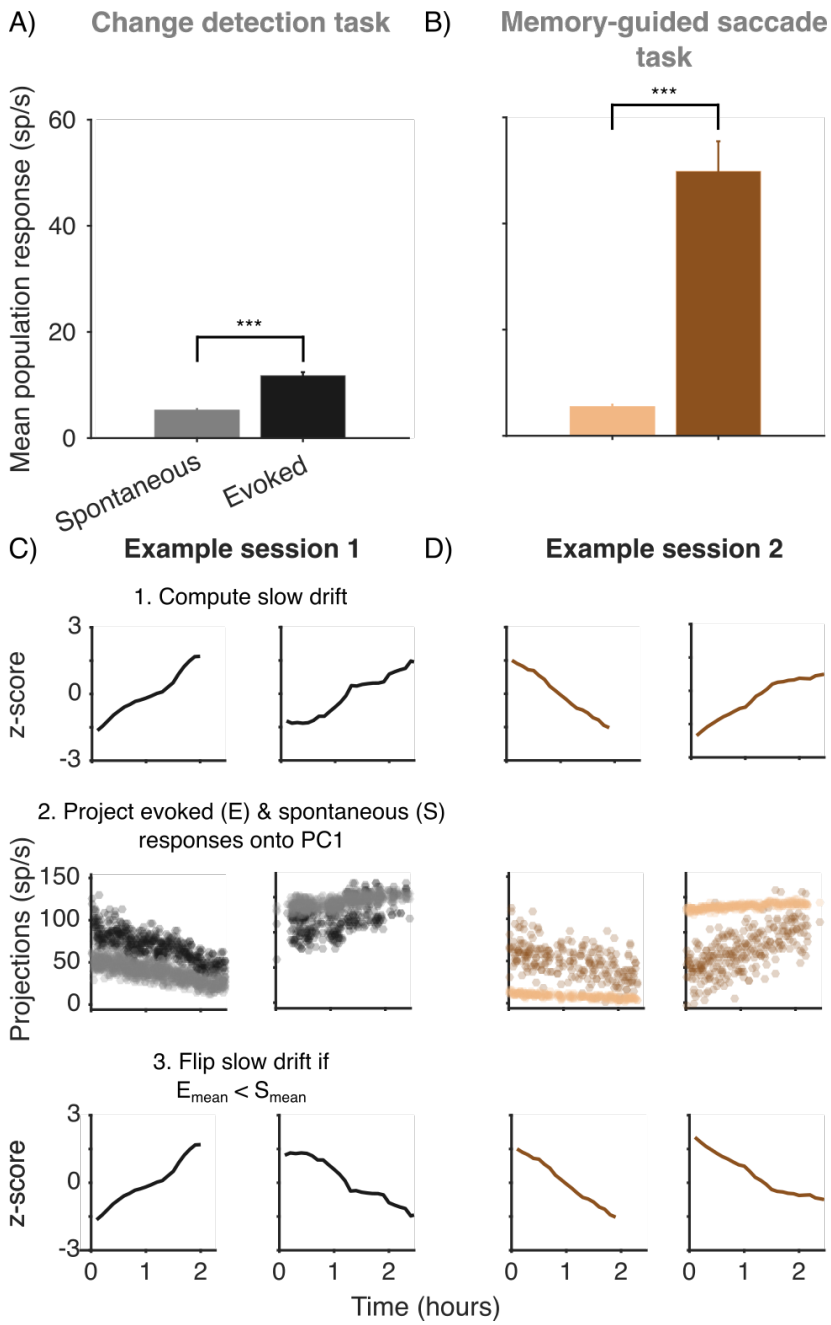

Figure S4. Aligning slow drift across sessions. (A) Bar charts showing the mean spontaneous and evoked population response across sessions on the change detection task. Spontaneous activity was calculated during fixation periods, whereas evoked activity was calculated during stimulus periods. (B) Same as (A) but for the memory-guided saccade task. Spontaneous activity was recorded during the delay period, whereas evoked activity was recorded during the presentation of the target stimulus. In (A) and (B) the mean evoked population response was significantly higher for evoked than spontaneous activity (two-sided permutation tests, difference of means). (C) For each session, slow drift on the change detection task was aligned by projecting evoked and spontaneous responses onto the first principal component. The sign of the slow drift was flipped if the mean projection value for the evoked responses was less than that for the spontaneous responses i.e., if the relationship shown in (A) for unprojected data did not hold true. (D) Same as (C) but for the memory-guided saccade task. $p < 0.05$*, $p < 0.01$**, $p < 0.001$***. Error bars represent ±1 SEM.

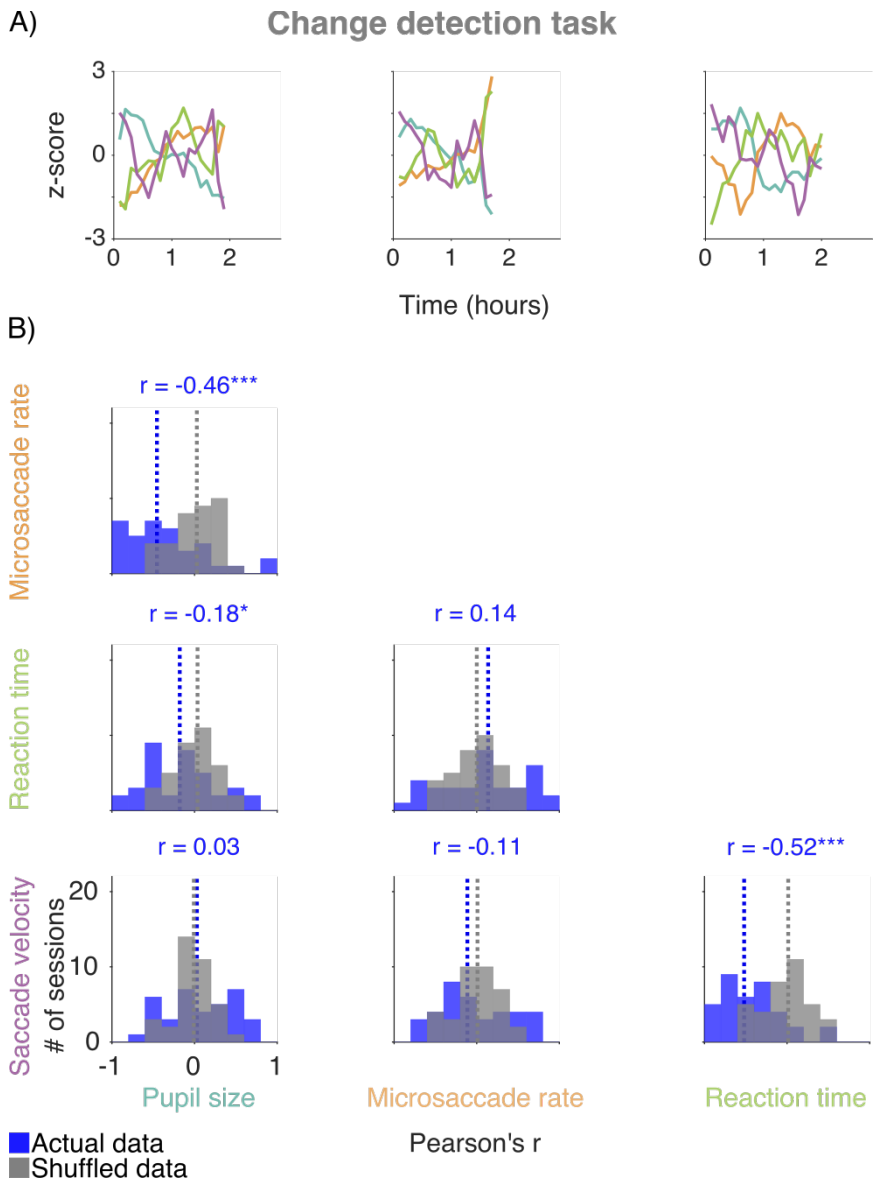

Figure S5. Correlations between the eye metrics on the change detection task. (A) Three example sessions from Monkey 1. (B) Histograms showing actual and shuffled distributions of r values across sessions. Median r values are indicated by dashed lines (blue lines = actual data; gray lines = shuffled data). Actual distributions of r values were compared to shuffled distributions using two-sided permutation tests (difference of medians). $p < 0.05$*, $p < 0.01$**, $p < 0.001$***.

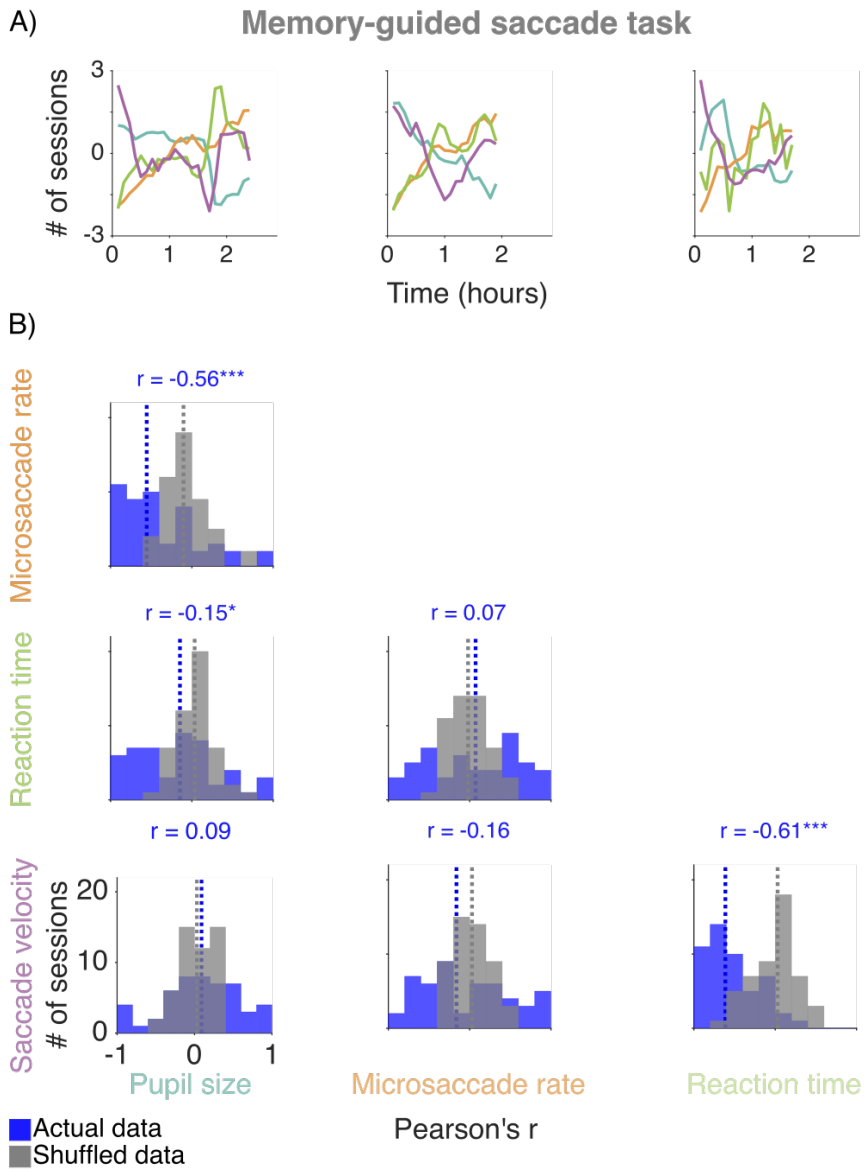

Figure S6. Correlations between the eye metrics on the memory-guided saccade task. (A) Three example sessions from Monkey 1. (B) Histograms showing actual and shuffled distributions of r values. Median r values are indicated by dashed lines (blue lines = actual data; gray lines = shuffled data). Actual distributions of r values were compared to shuffled distributions using two-sided permutation tests (difference of medians). $p < 0.05$*, $p < 0.01$**, $p < 0.001$***.

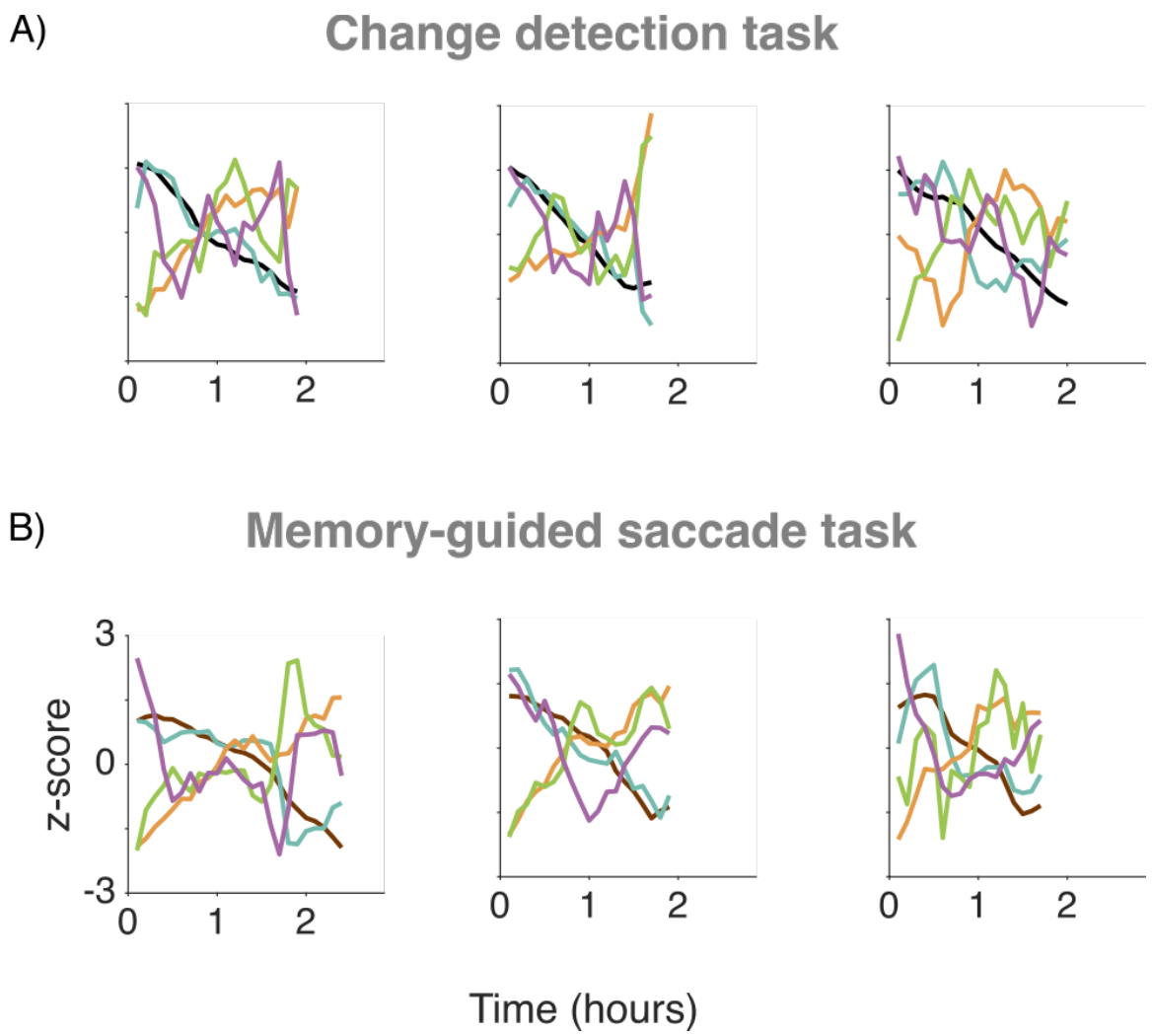

Figure S7. Correlations between slow drift and the eye metrics. (A) Three example sessions from Monkey 1 on the change detection task. (B) Same as (A) but for the memory-guided saccade task (same subject).

References

1. Hannula, D.E., Althoff, R.R., Warren, D.E., Riggs, L., Cohen, N.J., and Ryan, J.D. (2010). Worth a glance: Using eye movements to investigate the cognitive neuroscience of memory. Front. Hum. Neurosci. *4*, 1–16.
2. Ryan, J.D., and Shen, K. (2020). The eyes are a window into memory. Curr. Opin. Behav. Sci. *32*, 1–6. Available at: https://doi.org/10.1016/j.cobeha.2019.12.014.
3. König, P., Osnabrück, U., Ossandón, J.P., Ehinger, B. V, Osnabrück, U., Gameiro, R.R., Osnabrück, U., and Kaspar, K. (2016). Eye movements as a window to cognitive processes. J. Eye Mov. Res. *9*, 1–16.
4. Eckstein, M.K., Guerra-Carrillo, B., Miller Singley, A.T., and Bunge, S.A. (2017). Beyond eye gaze: What else can eyetracking reveal about cognition and cognitive development? Dev. Cogn. Neurosci. *25*, 69–91. Available at: http://dx.doi.org/10.1016/j.dcn.2016.11.001.
5. Aslin, R.N. (2012). Infant eyes: A window on cognitive development. Infancy *17*, 126–140.
6. Hessels, R.S., and Hooge, I.T.C. (2019). Eye tracking in developmental cognitive neuroscience – The good, the bad and the ugly. Dev. Cogn. Neurosci. *40*, 100710. Available at: https://doi.org/10.1016/j.dcn.2019.100710.
7. Rayner, K. (2009). Eye movements and attention in reading, scene perception, and visual search.
8. Di Stasi, L.L., Catena, A., Cañas, J.J., Macknik, S.L., and Martinez-Conde, S. (2013). Saccadic velocity as an arousal index in naturalistic tasks. Neurosci. Biobehav. Rev. *37*, 968–975.

9. Mathôt, S., and Van der Stigchel, S. (2015). New Light on the Mind's Eye: The Pupillary Light Response as Active Vision. Curr. Dir. Psychol. Sci. *24*, 374–378.

10. Larsen, R.S., and Waters, J. (2018). Neuromodulatory correlates of pupil dilation. Front. Neural Circuits *12*, 1–9.

11. Wang, C.A., and Munoz, D.P. (2015). A circuit for pupil orienting responses: Implications for cognitive modulation of pupil size. Curr. Opin. Neurobiol. *33*, 134–140. Available at: http://dx.doi.org/10.1016/j.conb.2015.03.018.

12. Joshi, S., and Gold, J.I. (2019). Pupil size as a window on neural substrates of cognition. Trends Cogn. Sci., 1–24. Available at: https://doi.org/10.1016/j.tics.2020.03.005.

13. Mathôt, S. (2018). Pupillometry: Psychology, Physiology, and Function. *1*, 1–23.

14. McCamy, M.B., Otero-Millan, J., Leigh, R.J., King, S.A., Schneider, R.M., Macknik, S.L., and Martinez-Conde, S. (2015). Simultaneous recordings of human microsaccades and drifts with a contemporary video eye tracker and the search coil technique. PLoS One *10*, 1–20.

15. Kimmel, D.L., Mammo, D., and Newsome, W.T. (2012). Tracking the eye non-invasively: Simultaneous comparison of the scleral search coil and optical tracking techniques in the macaque monkey. Front. Behav. Neurosci. *6*, 1–17.

16. Campbell, F.W., and Gregory, A.H. (1960). Effect of Size of Pupil on Visual Acuity. Nature *187*, 1121–1123.

17. Aston-Jones, G., and Cohen, J.D. (2005). AN INTEGRATIVE THEORY OF LOCUS COERULEUS-NOREPINEPHRINE FUNCTION: Adaptive Gain and Optimal Performance. Annu. Rev. Neurosci. *28*, 403–450.

18. van den Brink, R.L., Pfeffer, T., and Donner, T.H. (2019). Brainstem Modulation of

757 Large-Scale Intrinsic Cortical Activity Correlations. Front. Hum. Neurosci. *13*, 1–18.
758 19. Berridge, C.W., and Waterhouse, B.D. (2003). The locus coeruleus-noradrenergic system:
759 Modulation of behavioral state and state-dependent cognitive processes. Brain Res. Rev.
760 *42*, 33–84.
761 20. Sara, S.J. (2009). The locus coeruleus and noradrenergic modulation of cognition. Nat.
762 Rev. Neurosci. *10*, 211–223.
763 21. Samuels, E., and Szabadi, E. (2008). Functional Neuroanatomy of the Noradrenergic
764 Locus Coeruleus: Its Roles in the Regulation of Arousal and Autonomic Function Part II:
765 Physiological and Pharmacological Manipulations and Pathological Alterations of Locus
766 Coeruleus Activity in Humans. Curr. Neuropharmacol. *6*, 254–285.
767 22. Chandler, D.J. (2016). Evidence for a specialized role of the locus coeruleus noradrenergic
768 system in cortical circuitries and behavioral operations. Brain Res. *1641*, 197–206.
769 Available at: http://dx.doi.org/10.1016/j.brainres.2015.11.022.
770 23. Breton-Provencher, V., and Sur, M. (2019). Active control of arousal by a locus coeruleus
771 GABAergic circuit. Nat. Neurosci. *22*, 218–228. Available at:
772 http://www.ncbi.nlm.nih.gov/pubmed/30643295.
773 24. Schwarz, L.A., and Luo, L. (2015). Organization of the locus coeruleus-norepinephrine
774 system. Curr. Biol. *25*, R1051–R1056. Available at:
775 http://dx.doi.org/10.1016/j.cub.2015.09.039.
776 25. Szabadi, E. (2013). Functional neuroanatomy of the central noradrenergic system. J.
777 Psychopharmacol. *27*, 659–693.
778 26. Joshi, S., Li, Y., Kalwani, R.M., and Gold, J.I. (2016). Relationships between Pupil
779 Diameter and Neuronal Activity in the Locus Coeruleus, Colliculi, and Cingulate Cortex.

Neuron *89*, 221–234. Available at: http://dx.doi.org/10.1016/j.neuron.2015.11.028.

27. Varazzani, C., San-Galli, A., Gilardeau, S., and Bouret, S. (2015). Noradrenaline and dopamine neurons in the reward/effort trade-off: A direct electrophysiological comparison in behaving monkeys. J. Neurosci. *35*, 7866–7877.

28. Reimer, J., McGinley, M.J., Liu, Y., Rodenkirch, C., Wang, Q., McCormick, D.A., and Tolias, A.S. (2016). Pupil fluctuations track rapid changes in adrenergic and cholinergic activity in cortex. Nat. Commun. *7*, 1–7. Available at: http://dx.doi.org/10.1038/ncomms13289.

29. Kowler, E. (2011). Eye movements: The past 25years. Vision Res. *51*, 1457–1483. Available at: http://dx.doi.org/10.1016/j.visres.2010.12.014.

30. DiGirolamo, G.J., Patel, N., and Blaukopf, C.L. (2016). Arousal facilitates involuntary eye movements. Exp. Brain Res. *234*, 1967–1976.

31. Kristjánsson, Á., Vandenbroucke, M.W.G., and Driver, J. (2004). When pros become cons for anti- versus prosaccades: Factors with opposite or common effects on different saccade types. Exp. Brain Res. *155*, 231–244.

32. Castellote, J.M., Kumru, H., Queralt, A., and Valls-Solé, J. (2007). A startle speeds up the execution of externally guided saccades. Exp. Brain Res. *177*, 129–136.

33. Deuter, C.E., Schilling, T.M., Kuehl, L.K., Blumenthal, T.D., and Schachinger, H. (2013). Startle effects on saccadic responses to emotional target stimuli. Psychophysiology *50*, 1056–1063.

34. Rolfs, M. (2009). Microsaccades: Small steps on a long way. Vision Res. *49*, 2415–2441. Available at: http://dx.doi.org/10.1016/j.visres.2009.08.010.

35. Hafed, Z.M., Chen, C.-Y., and Tian, X. (2015). Vision, Perception, and Attention through

the Lens of Microsaccades: Mechanisms and Implications. Front. Syst. Neurosci. *9*, 1–16. Available at: http://journal.frontiersin.org/Article/10.3389/fnsys.2015.00167/abstract.

36. Martinez-Conde, S., Otero-Millan, J., and MacKnik, S.L. (2013). The impact of microsaccades on vision: Towards a unified theory of saccadic function. Nat. Rev. Neurosci. *14*, 83–96.

37. Gandhi, N.J., and Katnani, H.A. (2011). Motor Functions of the Superior Colliculus. Annu. Rev. Neurosci. *34*, 205–231. Available at: http://www.annualreviews.org/doi/10.1146/annurev-neuro-061010-113728.

38. Gao, X., Yan, H., and Sun, H.J. (2015). Modulation of microsaccade rate by task difficulty revealed through between- and within-trial comparisons. J. Vis. *15*, 1–15.

39. Siegenthaler, E., Costela, F.M., Mccamy, M.B., Di Stasi, L.L., Otero-Millan, J., Sonderegger, A., Groner, R., Macknik, S., and Martinez-Conde, S. (2014). Task difficulty in mental arithmetic affects microsaccadic rates and magnitudes. Eur. J. Neurosci. *39*, 287–294.

40. Valsecchi, M., Betta, E., and Turatto, M. (2007). Visual oddballs induce prolonged microsaccadic inhibition. Exp. Brain Res. *177*, 196–208.

41. Valsecchi, M., and Turatto, M. (2009). Microsaccadic responses in a bimodal oddball task. Psychol. Res. *73*, 23–33.

42. Reimer, J., Froudarakis, E., Cadwell, C.R., Yatsenko, D., Denfield, G.H., and Tolias, A.S. (2014). Pupil Fluctuations Track Fast Switching of Cortical States during Quiet Wakefulness. Neuron *84*, 355–362. Available at: http://dx.doi.org/10.1016/j.neuron.2014.09.033.

43. Leopold, D.A., and Logothetis, N.K. (1998). Microsaccades differentially modulate neural

826 activity in the striate and extrastriate visual cortex. Exp. Brain Res. *123*, 341–345.
827 44. Martinez-Conde, S., Macknik, S.L., and Hubel, D.H. (2000). Microsaccadic eye
828 movements and firing of single cells in the striate cortex of macaque monkeys. Nat.
829 Neurosci. *3*, 251–258.
830 45. Bair, W., and O'Keefe, L.R. (1998). The influence of fixational eye movements on the
831 response of neurons in area MT of the macaque. Vis. Neurosci. *15*, 779–786.
832 46. Snodderly, D.M., Kagan, I., and Moshe, G. (2001). Selective activation of visual cortex
833 neurons by fixational eye movements: Implications for neural coding. Vis. Neurosci. *18*,
834 259–277.
835 47. Herrington, T.M., Masse, N.Y., Hachmeh, K.J., Smith, J.E.T., Assad, J.A., and Cook, E.P.
836 (2009). The effect of microsaccades on the correlation between neural activity and
837 behavior in middle temporal, ventral intraparietal, and lateral intraparietal areas. J.
838 Neurosci. *29*, 5793–5805.
839 48. Chen, C.Y., Ignashchenkova, A., Thier, P., and Hafed, Z.M. (2015). Neuronal response
840 gain enhancement prior to microsaccades. Curr. Biol. *25*, 2065–2074. Available at:
841 http://dx.doi.org/10.1016/j.cub.2015.06.022.
842 49. Lowet, E., Gomes, B., Srinivasan, K., Zhou, H., Schafer, R.J., and Desimone, R. (2018).
843 Enhanced Neural Processing by Covert Attention only during Microsaccades Directed
844 toward the Attended Stimulus. Neuron *99*, 207-214.e3. Available at:
845 https://doi.org/10.1016/j.neuron.2018.05.041.
846 50. Steinmetz, N.A., and Moore, T. (2019). Changes in the Response Rate and Response
847 Variability of Area V4 Neurons During the Preparation of Saccadic Eye Movements.
848 1171–1178.

849 51. Khanna, S.B., Snyder, A.C., and Smith, M.A. (2019). Distinct sources of variability affect
850 eye movement preparation. J. Neurosci. *39*, 4511–4526.
851 52. Supèr, H., and Lamme, V.A.F. (2007). Strength of figure-ground activity in monkey
852 primary visual cortex predicts saccadic reaction time in a delayed detection task. Cereb.
853 Cortex *17*, 1468–1475.
854 53. Hanes, D.P., and Schall, J.D. (1996). Neural control of voluntary movement initiation.
855 Science (80-.). *274*, 427–430.
856 54. Cook, E.P., and Maunsell, J.H.R. (2002). Dynamics of neuronal responses in macaque MT
857 and VIP during motion detection. Nat. Neurosci. *5*, 985–994.
858 55. Roitman, J.D., and Shadlen, M.N. (2002). Response of neurons in the lateral intraparietal
859 area during a combined visual discrimination reaction time task. J. Neurosci. *22*, 9475–
860 9489.
861 56. Huang, X., and Lisberger, S.G. (2009). Noise correlations in cortical area MT and their
862 potential impact on trial-by-trial variation in the direction and speed of smooth-pursuit eye
863 movements. J. Neurophysiol. *101*, 3012–3030.
864 57. O'Leary, J.G., and Lisberger, S.G. (2012). Role of the lateral intraparietal area in
865 modulation of the strength of sensory-motor transmission for visually guided movements.
866 J. Neurosci. *32*, 9745–9754.
867 58. Cowley, B.R., Snyder, A.C., Acar, K., Williamson, R.C., Yu, B.M., and Smith, M.A.
868 (2020). Slow drift of neural activity as a signature of impulsivity in macaque visual and
869 prefrontal cortex. bioRxiv, 2020.01.10.902403. Available at:
870 https://www.biorxiv.org/content/10.1101/2020.01.10.902403v1.
871 59. Snyder, A.C., Yu, B.M., and Smith, M.A. (2018). Distinct population codes for attention

in the absence and presence of visual stimulation. Nat. Commun. *9*, 4382. Available at: http://www.nature.com/articles/s41467-018-06754-5.

60. Cowley, B.R., Snyder, A.C., Acar, K., Williamson, R.C., Yu, B.M., and Smith, M.A. (2018). The role that a slow drift in V4 population activity plays in perceptual decision-making.

61. Jollife, I.T., and Cadima, J. (2016). Principal component analysis: A review and recent developments. Philos. Trans. R. Soc. A Math. Phys. Eng. Sci. *374*.

62. Murray, J.D., Bernacchia, A., Roy, N.A., Constantinidis, C., Romo, R., and Wang, X.J. (2017). Stable population coding for working memory coexists with heterogeneous neural dynamics in prefrontal cortex. Proc. Natl. Acad. Sci. U. S. A. *114*, 394–399.

63. Harvey, C.D., Coen, P., and Tank, D.W. (2012). Choice-specific sequences in parietal cortex during a virtual-navigation decision task. Nature *484*, 62–68.

64. Mante, V., Sussillo, D., Shenoy, K. V., and Newsome, W.T. (2013). Context-dependent computation by recurrent dynamics in prefrontal cortex. Nature *503*, 78–84.

65. Wang, J., Narain, D., Hosseini, E.A., and Jazayeri, M. (2018). Flexible timing by temporal scaling of cortical responses. Nat. Neurosci. *21*, 102–112. Available at: http://dx.doi.org/10.1038/s41593-017-0028-6.

66. Sohn, H., Narain, D., Meirhaeghe, N., and Jazayeri, M. (2018). Bayesian computation through cortical latent dynamics. bioRxiv, 465419. Available at: https://www.biorxiv.org/content/early/2018/11/08/465419.

67. Remington, E.D., Narain, D., Hosseini, E.A., and Jazayeri, M. (2018). Flexible Sensorimotor Computations through Rapid Reconfiguration of Cortical Dynamics. Neuron *98*, 1005-1019.e5. Available at: https://doi.org/10.1016/j.neuron.2018.05.020.

68. Sadtler, P.T., Quick, K.M., Golub, M.D., Chase, S.M., Ryu, S.I., Tyler-Kabara, E.C., Yu, B.M., and Batista, A.P. (2014). Neural constraints on learning. Nature *512*, 423–426. Available at: http://dx.doi.org/10.1038/nature13665.

69. Stringer, C., Pachitariu, M., Steinmetz, N., Reddy, C.B., Carandini, M., and Harris, K.D. (2018). Spontaneous behaviors drive multidimensional, brain-wide population activity. bioRxiv *7893*, 306019. Available at: https://www.biorxiv.org/content/early/2018/12/28/306019?%3Fcollection=.

70. Williamson, R.C., Doiron, B., Smith, M.A., and Yu, B.M. (2019). Bridging large-scale neuronal recordings and large-scale network models using dimensionality reduction. Curr. Opin. Neurobiol. *55*, 40–47. Available at: https://doi.org/10.1016/j.conb.2018.12.009.

71. Cunningham, J.P., and Yu, B.M. (2014). Dimensionality reduction for large-scale neural recordings. Nat. Neurosci. *17*, 1500–1509.

72. Ruff, D.A., Ni, A.M., and Cohen, M.R. (2018). Cognition as a Window into Neuronal Population Space. Annu. Rev. Neurosci. *41*, 77–97.

73. Gallego, J.A., Perich, M.G., Miller, L.E., and Solla, S.A. (2017). Neural Manifolds for the Control of Movement. Neuron *94*, 978–984. Available at: http://dx.doi.org/10.1016/j.neuron.2017.05.025.

74. Waterhouse, B.D., and Chandler, D. (2012). Evidence for broad versus segregated projections from cholinergic and noradrenergic nuclei to functionally and anatomically discrete subregions of prefrontal cortex. Front. Behav. Neurosci. *6*, 1–9.

75. Chandler, D.J., Gao, W.J., and Waterhouse, B.D. (2014). Heterogeneous organization of the locus coeruleus projections to prefrontal and motor cortices. Proc. Natl. Acad. Sci. U. S. A. *111*, 6816–6821.

76. Cerpa, J.C., Marchand, A.R., and Coutureau, E. (2019). Distinct regional patterns in noradrenergic innervation of the rat prefrontal cortex. J. Chem. Neuroanat. *96*, 102–109. Available at: https://doi.org/10.1016/j.jchemneu.2019.01.002.

77. Schwarz, L.A., Miyamichi, K., Gao, X.J., Beier, K.T., Weissbourd, B., Deloach, K.E., Ren, J., Ibanes, S., Malenka, R.C., Kremer, E.J., *et al.* (2015). Viral-genetic tracing of the input-output organization of a central noradrenaline circuit. Nature *524*, 88–92.

78. Sharma, Y., Xu, T., Graf, W.M., Fobbs, A., Sherwood, C.C., Hof, P.R., Allman, J.M., and Manaye, K.F. (2010). Comparative anatomy of the locus coeruleus in humans and nonhuman primates. J. Comp. Neurol. *518*, 963–971.

79. German, D.C., and Bowden, D.M. (1975). Locus ceruleus in rhesus monkey (Macaca mulatta): A combined histochemical fluorescence, Nissl and silver study. J. Comp. Neurol. *161*, 19–29.

80. Kalwani, R.M., Joshi, S., and Gold, J.I. (2014). Phasic Activation of Individual Neurons in the Locus Ceruleus/Subceruleus Complex of Monkeys Reflects Rewarded Decisions to Go But Not Stop. J. Neurosci. *34*, 13656–13669.

81. Lehmann, S.J., and Corneil, B.D. (2016). Transient Pupil Dilation after Subsaccadic Microstimulation of Primate Frontal Eye Fields. J. Neurosci. *36*, 3765–3776.

82. Clayton, E.C., Rajkowski, J., Cohen, J.D., and Aston-Jones, G. (2004). Phasic activation of monkey locus ceruleus neurons by simple decisions in a forced-choice task. J. Neurosci. *24*, 9914–9920.

83. Aston-Jones, G., Rajkowski, J., and Kubiak, P. (1997). Conditioned responses of monkey locus coeruleus neurons anticipate acquisition of discriminative behavior in a vigilance task. Neuroscience *80*, 697–715.

941 84. Aston-Jones, G., Rajkowski, J., Kubiak, P., and Alexinsky, T. (1994). Locus coeruleus
942 neurons in monkey are selectively activated by attended cues in a vigilance task. J.
943 Neurosci. *14*, 4467–4480.
944 85. Hayat, H., Regev, N., Matosevich, N., Sales, A., Paredes-rodriguez, E., Krom, A.J.,
945 Bergman, L., Li, Y., Lavigne, M., Kremer, E.J., *et al.* (2020). Locus coeruleus
946 norepinephrine activity mediates sensory-evoked awakenings from sleep.
947 86. Carter, M.E., Yizhar, O., Chikahisa, S., Nguyen, H., Adamantidis, A., Nishino, S.,
948 Deisseroth, K., and De Lecea, L. (2010). Tuning arousal with optogenetic modulation of
949 locus coeruleus neurons. Nat. Neurosci. *13*, 1526–1535.
950 87. Li, Y., Hickey, L., Perrins, R., Werlen, E., Patel, A.A., Hirschberg, S., Jones, M.W.,
951 Salinas, S., Kremer, E.J., and Pickering, A.E. (2016). Retrograde optogenetic
952 characterization of the pontospinal module of the locus coeruleus with a canine adenoviral
953 vector. Brain Res. *1641*, 274–290. Available at:
954 http://dx.doi.org/10.1016/j.brainres.2016.02.023.
955 88. Quinlan, M.A.L., Strong, V.M., Skinner, D.M., Martin, G.M., Harley, C.W., and Walling,
956 S.G. (2019). Locus coeruleus optogenetic light activation induces long-term potentiation
957 of perforant path population spike amplitude in rat dentate gyrus. Front. Syst. Neurosci.
958 *12*, 1–14.
959 89. Liu, Y., Rodenkirch, C., Moskowitz, N., Schriver, B., and Wang, Q. (2017). Dynamic
960 Lateralization of Pupil Dilation Evoked by Locus Coeruleus Activation Results from
961 Sympathetic, Not Parasympathetic, Contributions. Cell Rep. *20*, 3099–3112. Available at:
962 https://doi.org/10.1016/j.celrep.2017.08.094.
963 90. Vazey, E.M., and Aston-Jones, G. (2014). Designer receptor manipulations reveal a role

964 of the locus coeruleus noradrenergic system in isoflurane general anesthesia. Proc. Natl.
965 Acad. Sci. U. S. A. *111*, 3859–3864.
966 91. Massot, C., Jagadisan, U.K., and Gandhi, N.J. (2019). Sensorimotor transformation elicits
967 systematic patterns of activity along the dorsoventral extent of the superior colliculus in
968 the macaque monkey. Commun. Biol. *2*, 1–14. Available at:
969 http://dx.doi.org/10.1038/s42003-019-0527-y.
970 92. Sparks, D.L., and Hartwich-Young, R. (1989). The deep layers of the superior colliculus.
971 Rev. Oculomot. Res. *3*, 213–255.
972 93. Kaufman, M.T., Churchland, M.M., Ryu, S.I., and Shenoy, K. V. (2014). Cortical activity
973 in the null space: Permitting preparation without movement. Nat. Neurosci. *17*, 440–448.
974 94. Elsayed, G.F., Lara, A.H., Kaufman, M.T., Churchland, M.M., and Cunningham, J.P.
975 (2016). Reorganization between preparatory and movement population responses in motor
976 cortex. Nat. Commun. *7*, 1–15. Available at: http://dx.doi.org/10.1038/ncomms13239.
977 95. Ames, K.C., and Churchland, M.M. (2019). Motor cortex signals corresponding to the two
978 arms are shared across hemispheres, mixed among neurons, yet partitioned within the
979 population response. bioRxiv, 1–45.
980 96. Stavisky, S.D., Kao, J.C., Ryu, S.I., and Shenoy, K. V. (2017). Motor Cortical Visuomotor
981 Feedback Activity Is Initially Isolated from Downstream Targets in Output-Null Neural
982 State Space Dimensions. Neuron *95*, 195-208.e9. Available at:
983 http://dx.doi.org/10.1016/j.neuron.2017.05.023.
984 97. Wang, C.-A., Baird, T., Huang, J., Coutinho, J.D., Brien, D.C., and Munoz, D.P. (2018).
985 Arousal Effects on Pupil Size, Heart Rate, and Skin Conductance in an Emotional Face
986 Task. Front. Neurol. *9*, 1–13.

987 98. Samaha, J., Iemi, L., and Postle, B.R. (2017). Prestimulus alpha-band power biases visual
988 discrimination confidence, but not accuracy. Conscious. Cogn. *54*, 47–55. Available at:
989 http://dx.doi.org/10.1016/j.concog.2017.02.005.
990 99. Benwell, C.S.Y., Tagliabue, C.F., Veniero, D., Cecere, R., Savazzi, S., and Thut, G.
991 (2017). Prestimulus EEG power predicts conscious awareness but not objective visual
992 performance. eNeuro *4*, 1–17.
993 100. Romei, V., Gross, J., and Thut, G. (2010). On the role of prestimulus alpha rhythms over
994 occipito-parietal areas in visual input regulation: Correlation or causation? J. Neurosci. *30*,
995 8692–8697.
996 101. Van Dijk, H., Schoffelen, J.M., Oostenveld, R., and Jensen, O. (2008). Prestimulus
997 oscillatory activity in the alpha band predicts visual discrimination ability. J. Neurosci. *28*,
998 1816–1823.
999 102. Bellet, J., Chen, C.Y., and Hafed, Z.M. (2017). Sequential hemifield gating of α-and β-
1000 behavioral performance oscillations after microsaccades. J. Neurophysiol. *118*, 2789–
1001 2805.
1002 103. Engbert, R., and Kliegl, R. (2003). Microsaccades uncover the orientation of covert
1003 attention. Vision Res. *43*, 1035–1045.
1004 104. Hafed, Z.M. (2013). Alteration of Visual Perception prior to Microsaccades. Neuron *77*,
1005 775–786. Available at: http://dx.doi.org/10.1016/j.neuron.2012.12.014.
1006 105. Hafed, Z.M., and Clark, J.J. (2002). Microsaccades as an overt measure of covert attention
1007 shifts. Vision Res. *42*, 2533–2545.
1008 106. Rolfs, M., Engbert, R., and Kliegl, R. (2005). Crossmodal coupling of oculomotor control
1009 and spatial attention in vision and audition. Exp. Brain Res. *166*, 427–439.

107. Laubrock, J., Engbert, R., and Kliegl, R. (2005). Microsaccade dynamics during covert attention. Vision Res. *45*, 721–730.

108. Smith, M.A., and Sommer, M.A. (2013). Spatial and Temporal Scales of Neuronal Correlation in Visual Area V4. J. Neurosci. *33*, 5422–5432. Available at: http://www.jneurosci.org/cgi/doi/10.1523/JNEUROSCI.4782-12.2013.

109. Rabinowitz, N.C., Goris, R.L., Cohen, M., and Simoncelli, E.P. (2015). Attention stabilizes the shared gain of V4 populations. Elife *4*, 1–24.

110. Shoham, S., Fellows, M.R., and Normann, R.A. (2003). Robust, automatic spike sorting using mixtures of multivariate t-distributions. J. Neurosci. Methods *127*, 111–122.

111. Kelly, R.C., Smith, M.A., Samonds, J.M., Kohn, A., Bonds, A.B., Movshon, J.A., and Sing Lee, T. (2007). Comparison of Recordings from Microelectrode Arrays and Single Electrodes in the Visual Cortex. J. Neurosci. *27*, 261–264.

112. Brainard, D.H. (1997). The Psychophysics Toolbox. Spat. Vis. *10*, 433–436.

113. Pelli, D.G. (1997). The VideoToolbox software for visual psychophysics: Transforming numbers into movies. Spat. Vis. *10*, 437–442.

114. Scholes, C., McGraw, P. V., Nyström, M., and Roach, N.W. (2015). Fixational eye movements predict visual sensitivity. Proc. R. Soc. B Biol. Sci. *282*.

115. Loughnane, G.M., Newman, D.P., Tamang, S., Kelly, S.P., and O'Connell, R.G. (2018). Antagonistic interactions between microsaccades and evidence accumulation processes during decision formation. J. Neurosci. *38*, 2163–2176.

116. Zuber, B.L., Stark, L., and Cook, G. (1965). Microsaccades and the velocity-amplitude relationship for saccadic eye movements. Science (80-.). *150*, 1459–1460.